Ocean Engineering 326 (2025) 120917

Contents lists available at ScienceDirect

Ocean Engineering

journal homepage: www.elsevier.com/locate/oceaneng

Research paper

Combining Conv-LSTM and wind-wave data for enhanced sea wave forecasting in the Mediterranean Sea

P. Scala *, G. Manno, E. Ingrassia, G. Ciraolo

Department of Engineering, University of Palermo, 90128, Palermo, Italy

ARTICLE INFO

Keywords:
Sea-waves modeling
Deep learning techniques
Regional scale
CMEMS wave/wind data
Wave buoy

ABSTRACT

This study presents an application of a stateful Convolutional Long Short-Term Memory (Conv-LSTM) model for wave forecasting in the Mediterranean Sea. By leveraging bathymetric data and wind fields, the model predicts key oceanographic variables such as significant wave height (H_s), peak period (T_p), and wave direction (θ). By incorporating wave buoy measurements into the training data, the Conv-LSTM model effectively captures both spatial and temporal dynamics, particularly in regions characterised by complex wind-wave interactions. While the model shows high accuracy in predicting short-term wave variability, especially in central Mediterranean areas, it exhibits limitations in coastal regions under extreme weather conditions, where local factors and missing variables (e.g., air pressure, air temperature) reduce its accuracy (from 90% to 78%). Validation of measured data confirms the potential of the model to improve operational forecasting, maritime safety, and offshore engineering projects and highlights the need for improving spatial resolution and the inclusion of additional meteorological inputs for future applications.

1. Introduction

The Mediterranean is a semi-enclosed basin of great socioeconomic and environmental importance, characterised by unique and complex oceanographic conditions (Azzopardi et al., 2020; Danovaro et al., 2020; Lionello et al., 2006; Lloret et al., 2022; Salhi et al., 2021). Accurate modeling of wave conditions in this region is crucial for a wide range of applications, from maritime safety and coastal resource management to the energy industry and climate change risk mitigation (Bolaños-Sanchez et al., 2007; Cavaleri et al., 2010, 2018; Sartini et al., 2017).

Traditionally, wave forecasting has been carried out using physical-mathematical models such as spectral wave models, including well-known models such as WAM (Group, 1988; Komen, 1986), SWAN (Booij et al., 1999), and WaveWatch III (Tolman, 1991). These models are based on the solution of the wave action balance equation and are widely used for operational wave forecasting due to their ability to simulate wave growth, propagation, and dissipation over large domains. For example, WAM, was one of the first models to successfully integrate the effects of wind input, wave-wave interactions, and dissipation, whereas SWAN, developed later, allows for detailed wave modelling in coastal areas with complex bathymetry. WaveWatch III, an evolution of the earlier models, has become one of the standard tools for global and regional wave predictions, widely applied in both research and operational environments. These models have been further refined and validated through numerous studies, helping to improve the accuracy of wave forecasting in various marine environments. Although these models are robust and well-established, they have limitations, especially in terms of their spatial resolution and ability to represent the complexity of non-linear interactions between waves and meteorological conditions on a regional scale (Casaioli et al., 2014; Cavaleri et al., 2012, 2018; Hewitt et al., 2017; Sherwood et al., 2022; Toimil et al., 2020). Wave forecasting in the Mediterranean Sea is particularly challenging due to its semi-enclosed nature, seasonal variability, and the influence of local winds (Barceló-Llull et al., 2019; Denaxa et al., 2024; Mariotti et al., 2015). According to Tintoré et al. (2019), the Mediterranean is especially vulnerable to the impacts of climate change, including alterations in thermohaline circulation, extreme wave heights, and warming, all of which affect wave dynamics. Furthermore, Ravdas et al. (2018) emphasize that the complexity of the basin necessitates high-resolution forecasting systems to accurately capture local wave conditions. Seasonal variability and local wind influences introduce additional challenges, making detailed modeling essential for reliable predictions. However, traditional models often struggle to accurately

* Corresponding author.
E-mail address: pietro.scala@unipa.it (P. Scala).

https://doi.org/10.1016/j.oceaneng.2025.120917
Received 11 November 2024; Received in revised form 3 March 2025; Accepted 7 March 2025
Available online 12 March 2025
0029-8018/© 2025 The Authors. Published by Elsevier Ltd. This is an open access article under the CC BY license (http://creativecommons.org/licenses/by/4.0/).

capture these intricate dynamics.

Recently, the application of artificial intelligence-based approaches, in detail neural networks and deep learning models, has shown promising results in the field of marine and coastal engineering (Scala et al., 2024a, 2024b; Wang et al., 2022; Zhou et al., 2020) and especially in wave forecasting which can improve the representation of temporal and spatial variability of waves (Bento et al., 2021; Habib and Zarillo, 2024; Zhang and Li, 2020; Zheng et al., 2020).

In this context, Convolutional Long Short-Term Memory (Conv-LSTM) models provide a particularly suitable framework for predicting time series with strong spatial dependencies, such as sea wave motion (Hu et al., 2023; Upreti et al., 2023; Wang et al., 2021). Conv-LSTM models are designed to capture not only temporal, but also spatial dynamics, combining the capabilities of convolutional networks to extract spatial features with the ability of LSTMs to model long-term temporal dependencies (Shi et al., 2015). Several studies have demonstrated the effectiveness of such approaches in predicting of complex atmospheric and marine phenomena, such as weather conditions (O'Donncha et al., 2022; Shi et al., 2015) and waves (Ding et al., 2023; Hu et al., 2023; Liu et al., 2023; Ouyang et al., 2023; Upreti et al., 2023), suggesting that they can be a powerful tool to improve the prediction of weather and sea conditions in areas of high interest such as the Mediterranean Sea.

Despite these considerations, to the best of our knowledge, only a limited number of previous studies have applied the Conv-LSTM model for wave forecasting in the Mediterranean Sea. Prior research has primarily focused on traditional neural network-based approaches or deterministic models (Ducournau and Fablet, 2016; Oppenheim et al., 2019; Wu et al., 2019), without fully leveraging the spatiotemporal learning capabilities of Conv-LSTM. However, recent studies have explored alternative deep learning techniques for forecasting oceanographic conditions in the Mediterranean.

For instance, Neshat et al. (2022) proposed a decomposition-based Bi-LSTM model optimized with the Nelder-Mead algorithm, demonstrating improved wave power forecasting capabilities offshore of Favignana Island, with a 6-h prediction horizon. Similarly, Accarino et al. (2021) developed a multi-model LSTM architecture for sea level prediction in the Southern Adriatic Northern Ionian (SANI) domain of the Mediterranean, emphasizing the importance of long-term memory in capturing temporal variations and concluding that the LSTM-based approach outperforms physics-driven models.

Krestenitis et al. (2024) applied deep learning techniques for sea surface temperature forecasting in the Aegean, Ionian, and Cretan Seas, demonstrating the model's effectiveness in predicting thermal anomalies and marine heatwaves. Their approach proved particularly suitable for accurate spatiotemporal forecasting across multiple regions simultaneously, without the need for separate models for each subregion.

Regarding wave forecasting, Dakar et al. (2023) employed an artificial neural network (ANN) to predict wave height at a specific wave measurement station along Israel's Mediterranean coast, integrating wind data with wave observations. Their results indicated improvements over traditional models, particularly in estimating wave heights exceeding 1.5 m, where the ANN outperformed the SWAN wave model. Finally, Zhang et al. (2024) enhanced wave height prediction using a CNN-LSTM model, highlighting the potential of combining convolutional and recurrent networks for oceanographic forecasting. Their model was applied in a localized Mediterranean area, specifically near the mouth of the Yangtze River (126°E, 30°N).

In this paper, we propose the application of a Conv-LSTM model for wave prediction at the scale of the whole Mediterranean basin, using bathymetric data and wind fields (easterly and northerly components) as inputs as proposed by Song et al. (2022), Feng et al. (2022) Li et al. (2024). The model was trained to predict three fundamental variables for describing the sea state: significant wave height (H_s), peak period (Tp) and wave direction (θ). These quantities, essential for characterising wave dynamics, are widely used in sea state modeling and forecasting (Cañellas et al., 2024; Zheng et al., 2023).

The results show how the proposed approach can provide accurate predictions, in some cases exceeding the performance of CMEMS (Copernicus Marine Environment Monitoring Service) model, particularly in situations where the complexity of local interactions between wind and bathymetric features plays a crucial role. Our work is part of a line of research that aims to harness the increasing availability of high-resolution data and the power of machine learning tools to improve the prediction of sea state conditions at regional level (Ding et al., 2023; Donnelly et al., 2024; Jörges et al., 2023).

Following this initial introductory section, the paper is structured as follows: Section two details the data used, the CMEMS wave and wind data and the measured wave data. Section three describes the methods, focusing on the description of the model, architecture and the parameters used, as well as the optimization function and error and accuracy metrics for evaluating model performance. Section four presents the results of the training and validation phases and the results and discussion of the applications of the model in the context of the Mediterranean on CMEMS data and with respect to measured data from wave buoys in Italy. A comparison section with the currently presented models and approaches is also present in the discussions section. Finally, Section 5 offers the main conclusions of the study.

2. Materials

2.1. CMEMS waves and winds dataset

The Conv-LSTM model has been used to predict time series of waves characteristics based on forcing data as eastward and northward wind (height 10-m) data (m/s) and bathymetry for the whole Mediterranean Sea. This study has been conducted using E.U. Copernicus Marine Service Information datasets. The model was trained with a robust and valuable dataset of waves, in particular H_s, Tp, θ (https://doi.org/10.25423/cmcc/medsea_multiyear_wav_006_012), wind (https://doi.org/10.48670/moi-00185) and bathymetric data belonging to the Copernicus service. The Copernicus Marine Environment Monitoring Service (CMEMS) or Copernicus Marine Service (CMS) provides free and open access data and information related to the physical state of the global atmosphere and ocean. Hourly wave, bathymetric and wind data were downloaded using the web interface provided by CMEMS (last accessed on June 20, 2024) in netCDF format with, imposing a regional domain as shown in Fig. 1 (**subplot A**). The wave product is obtained using a WAM 4.6.2 model, provided by the Hellenic Centre for Marine Research (HCMR), in Greece, using a regular grid with a spatial resolution of 1/24° (approximately 4.6 km). The wind product is provided by the Royal Netherlands Meteorological Institute (KNMI) based on near real time and multi-year wind observations from scatterometers and on numerical weather prediction model fields, with a spatial resolution of 1/8°. The scatterometer products from the EUMETSAT Ocean and Sea Ice Satellite Application Facility have been extensively validated (Kokkos et al., 2021). Since the grid resolution of the models are different, as shown in Fig. 1 (**subplot B**), a data preprocessing was needed to resample the wind data with a wave grid spatial resolution using a triangular linear interpolation.

2.2. RON buoy data

The Italian Institute for Environmental Protection and Research, ISPRA (*Istituto Superiore per la Protezione e la Ricerca Ambientale*) is the national institute that is on charge, among other activities, to manage, collect the data and maintain the national wave buoy network (*Rete Ondametrica Nazionale*, RON). The network, after a maximum expansion period, is now composed by 9 wave buoys, equipped with different instrument as accelerometers, meteorological station and GPS (Fig. 2). All wave data area free available from the main ISPRA sea data dedicated web page (https://www.mareografico.it/en/homepage.html).

To evaluate the effectiveness in model training between measured

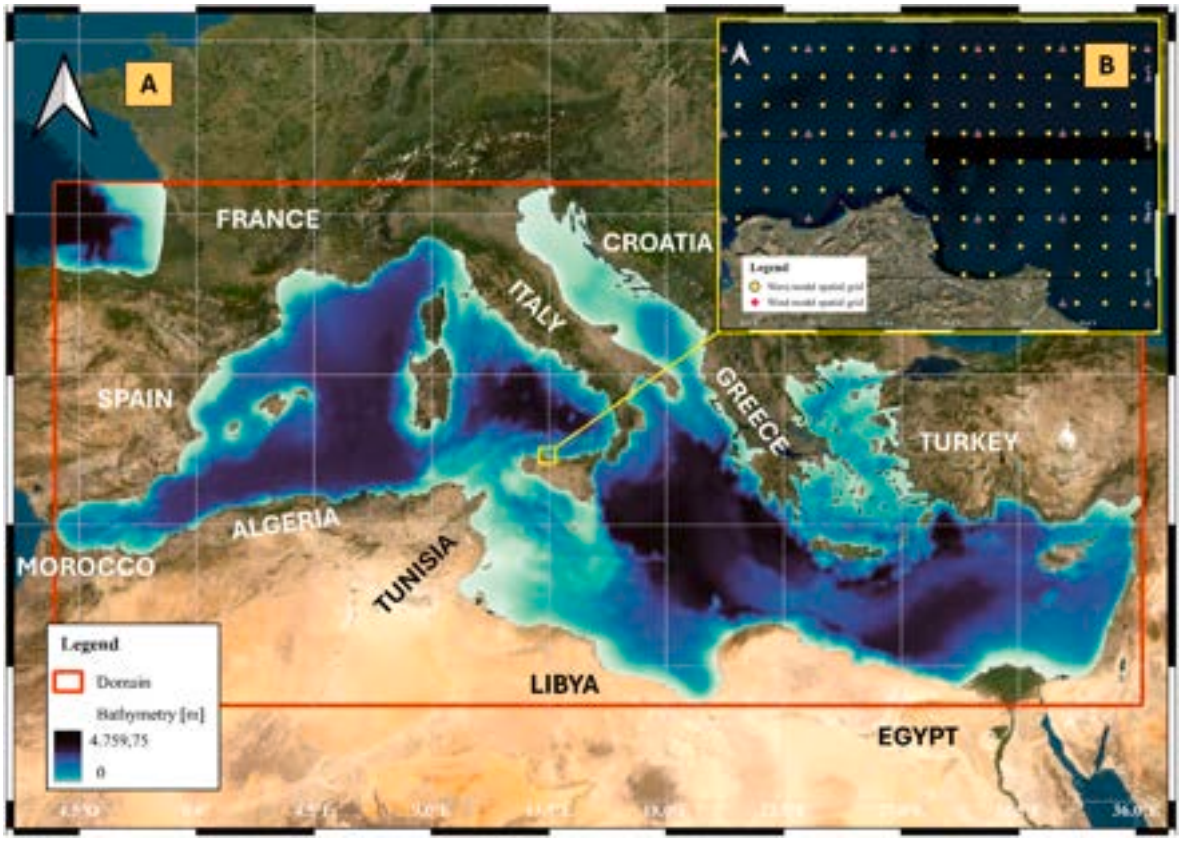

Fig. 1. Study Area and Dataset Grid Resolution. The regional domain used for the study is highlighted in red, covering the entire Mediterranean Sea (subpolot A). Subplot B is a Zoomed-in view showing the different grid resolutions of the CMEMS datasets. System Reference: WGS 84 Pseudo-Mercator EPSG 3857. (For interpretation of the references to colour in this figure legend, the reader is referred to the Web version of this article.)

Fig. 2. ISPRA RON buoy network. Buoy data used are shown in yellow, while those not used are shown in red (System Reference: WGS 84 Pseudo-Mercator EPSG 3857). (For interpretation of the references to colour in this figure legend, the reader is referred to the Web version of this article.)

Table 1
Dates of the events used for further validation model.

Period	Date	Short description
1	20-09-2020	The effect of Ianos Medicane affecting the eastern part of the Mediterranean basin
2	28-11-2021	Strong windstorm effect entering from Gulf of Lion through the central part of the Mediterranean basin
3	11-07-2022	Summer conditions in the basin with localized and low energetic Sirocco and Mistral winds
4	27-01-2022	Winter conditions brought a typical wave condition not related to Medicanes or extreme event

(RON) and simulated (CMEMS) data, we substituted all available H_s, Tp, and θ data measured by RON for the corresponding CMEMS domain calculation cells. In detail, Mazara del Vallo, Alghero, La Spezia, Ponza, Monopoli and Crotone buoys since 1993 and Ancona since march1999.

For the dates/periods when the buoys did not work or were under maintenance (so there were no acquisitions) we kept CMEMS data.

The Conv-LSTM was first compared with the CMEMS data model, and then with the buoy data from the RON to obtain an estimate of local accuracy. Four different 24-h events, shown in Table 1, were selected to validate the model.

We chose the events shown in Table 1 to test the model under heterogeneous conditions, considering both stormier (both wind and sea) and calmer scenarios. In particular, on 20 September 2020, the Mediterranean was still under the influence of Medicane Ianos, a powerful tropical cyclone that had swept through the region earlier in the month. The storm primarily hit Greece, with sustained winds reaching up to 40 m *per* second (144 km/h) and causing severe storm surges along the eastern Mediterranean coasts. Coastal areas in Greece experienced significant flooding due to the combination of high winds and high sea levels.

By 26 November 2021, the Mediterranean was recovering from the impact of Cyclone Apollo, which had brought strong winds and heavy rains to the central Mediterranean in late October and early November. Apollo had mainly affected areas such as Sicily and Malta, leaving rough seas conditions and localised flooding in its wake. Although the cyclone had dissipated by the end of November, the region is likely to have experienced residual unsettled weather with moderate winds and waves.

In contrast, the weather on July 11, 2022, was typical of the Mediterranean summer, characterised by generally calm seas and stable conditions. While no significant cyclones or storms were recorded during this period, localised winds such as the Mistral or Sirocco, which are common in the Mediterranean during the summer, may have caused occasional periods of increased wind and waves. However, the overall sea conditions were likely relatively tranquil compared to other dates.

Finally, by 27 January 2022, the Mediterranean was experiencing strong winter storms linked to extratropical cyclones. These winter

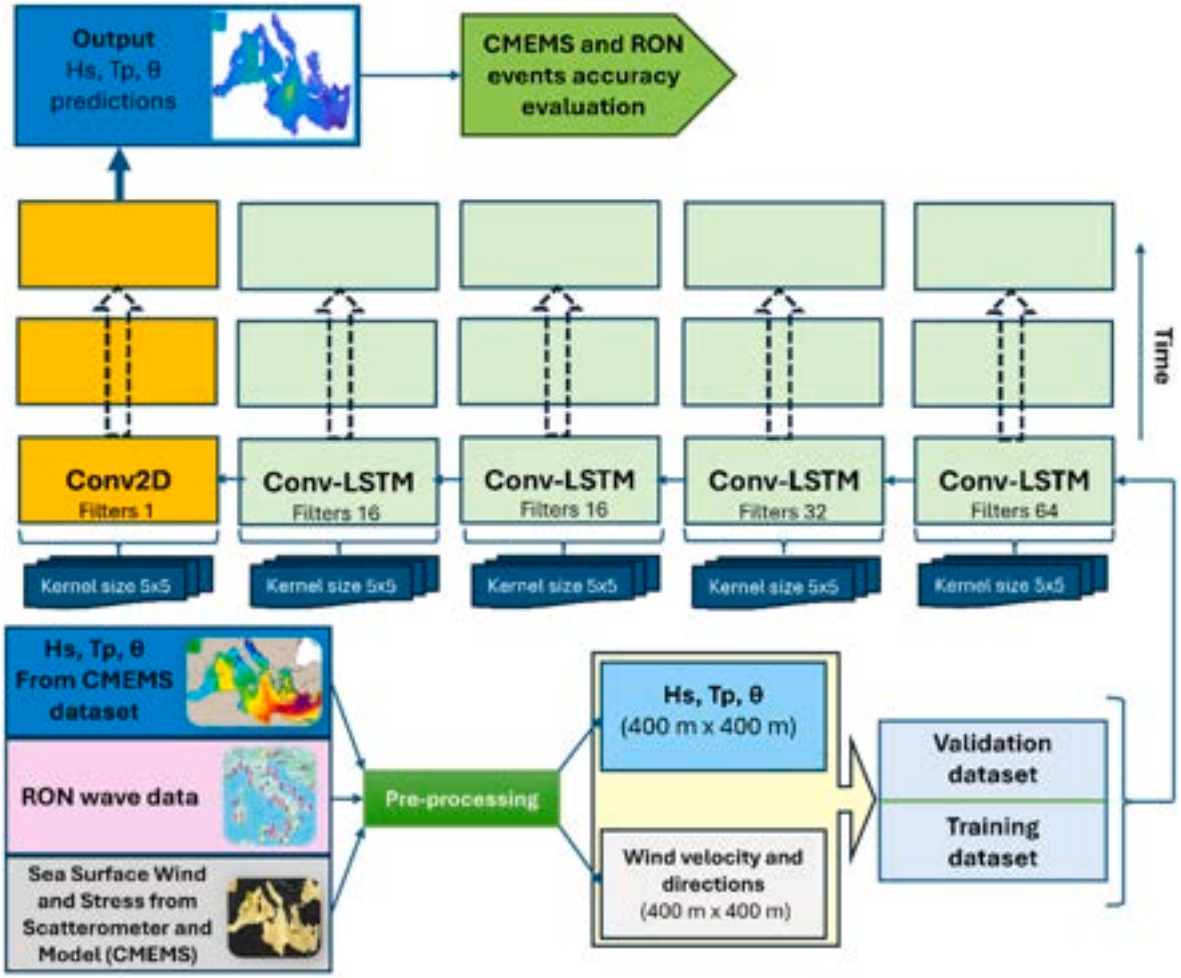

Fig. 3. Schematic representation of the Conv-LSTM model architecture for wave characteristics prediction in the Mediterranean Sea. The model is fed with wind velocity and directions, and wave data (significant wave height H_s, peak period Tp, and wave direction θ) obtained from the CMEMS dataset, as well as RON buoy data for validation. Input data undergoes pre-processing to match spatial resolution (400m × 400m). The network consists of Conv2D and sequential Conv-LSTM layers, with progressively increasing filters and kernel sizes of 5x5. The final output is the predicted H_s, Tp, and θ, with an accuracy evaluation performed using CMEMS and RON events.

systems are often accompanied by intense winds and rough seas, especially in the western part of the basin. As a result, maritime conditions would have been rough, with elevated wave heights and dangerous seas, typical of winter storms in the region.

3. Methods

3.1. Model description

A model based on Convolutional Long Short-Term Memory (Conv-LSTM) neural networks (Fu et al., 2022) has been developed to predict wave height, period and direction in the Mediterranean Sea. This model integrates spatial and temporal information from wind and bathymetry datasets to predict wave characteristics 24 h in advance. The architecture and simulation processes of the model are described in the following sections. A graphic visualisation of the workflow is shown in Fig. 3.

3.1.1. Model input

Model inputs include wind data, which are provided on a fine resolution spatial grid, representing wind speed and direction over the entire surface of the Mediterranean Sea, and bathymetry data, which represent seabed depth, a key variable influencing wave formation and behavior.

The wind data are pre-processed to produce spatial maps on which convolutions are applied. The bathymetry data, which is stationary in time, are combined with the wind maps to provide the model with geophysical context.

3.1.2. Model architecture

The architecture of the Conv-LSTM model (Hashmi et al., 2020) consists of several layers, each of which has a specific role:

The first is Convolutional Layers (Conv) which are used to extract spatial features from wind and bathymetry maps. The Conv(X, W) convolution is defined as Eq. (1):

$$Y_{i,j,k} = \sum_{p=0}^{P-1} \sum_{q=0}^{Q-1} X_{i+p,j+q,a}\, W_{p,q,a,k} \qquad \text{(Eq. 1)}$$

where X is the input (wind maps and bathymetry), W is the convolutional kernel, and Y is the convolutional output. More specifically, $Y_{i,j,k}$ is the element of the output tensor located at position (i,j) of channel k. $Y_{i,j,k}$ thus represents the value obtained after applying convolution to the portion of the input image and the filter associated with channel k.

$X_{i+p,j+q,a}$ is the input tensor element located at position $(i+p, j+q)$ of channel a. The input tensor X is the two-channel wind map (wind in x direction and wind in y direction).

$W_{p,q,a,k}$ is the element of the convolution kernel (filter) located at position (p,q) between channels a (input channel) and k (output channel). The filter W has size P x Q and is applied to all channels a of the input to produce channel k of the output.

The summations $\sum_{p=0}^{P-1} \sum_{q=0}^{Q-1}$ are double sums that iterate over the indices p and q respectively, which run over the values of the kernel window W that is applied to the input tensor X.

To capture the temporal dynamics of the wave features, the model uses LSTM layers applied to the spatial feature maps produced by the convolutional layers. The temporal dynamics is modelled by a combination of memory cells and LSTM gates, with the following equations (from 2 to 6):

$$f_t = \sigma\left(W_f\,[h_{t-1}, x_t] + b_f\right) \qquad \text{(Eq. 2)}$$

$$i_t = \sigma(W_i\,[h_{t-1}, x_t] + b_i) \qquad \text{(Eq. 3)}$$

$$C_t = f_t\, C_{t-1} + i_t \tanh\left(W_C\,[h_{t-1}, X_t] + b_C\right) \qquad \text{(Eq. 4)}$$

$$\partial_t = \sigma(W_\partial\,[h_{t-1}, x_t] + b_\partial) \qquad \text{(Eq. 5)}$$

$$h_t = \partial_t \tanh\,(C_t) \qquad \text{(Eq. 6)}$$

where ft, it, Ct, δt, and ht represent the forgetting gate, input gate, cell state, output gate and hidden output at time t respectively.

More specifically, the forgetting gate determines how much of the past information should be retained or forgotten.

The Input Gate decides which new information updates the cell state, the Cell State stores the important information that needs to be remembered over time, the Output Gate regulates how much of the stored information is to be used to generate the output at the current time, and the Hidden Output identifies the final representation of the LSTM cell that will be used for predictions or to pass information to the next time step.

More information on all terms in the equations can be found in the supplementary materials.

The model was configured with *stateful=True* (Ghasemirahni et al., 2024; Khan et al., 2019), which means that the hidden state and cell state of the LSTM are maintained between batches during training or inference, rather than being reset. This is useful when dealing with long training sequences or with data that is split into batches but represents a single continuous sequence as in the present work. An example of what a stateful LSTM architecture looks like is shown in Fig. 4.

Specifically, in a traditional (non-stateful) LSTM network, the hidden state (ht) and cell state (Ct) are initially reset after each batch. In a

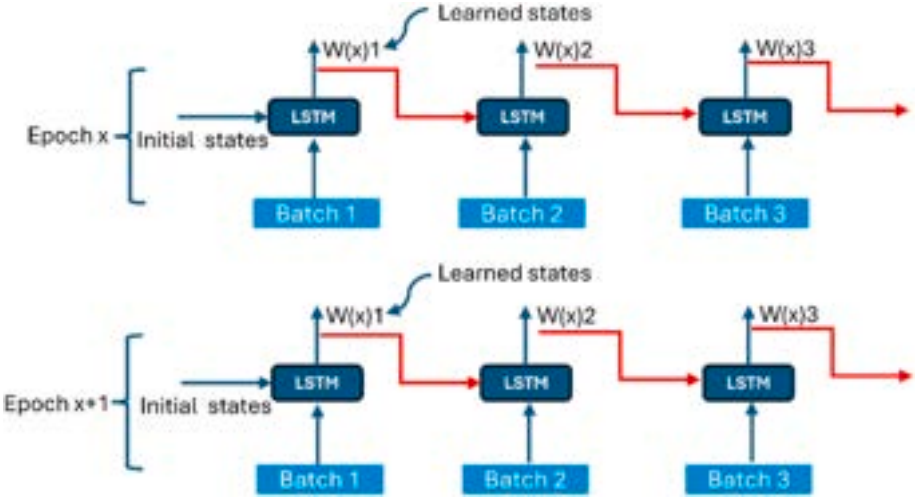

Fig. 4. Schematic representation of a stateful LSTM architecture.

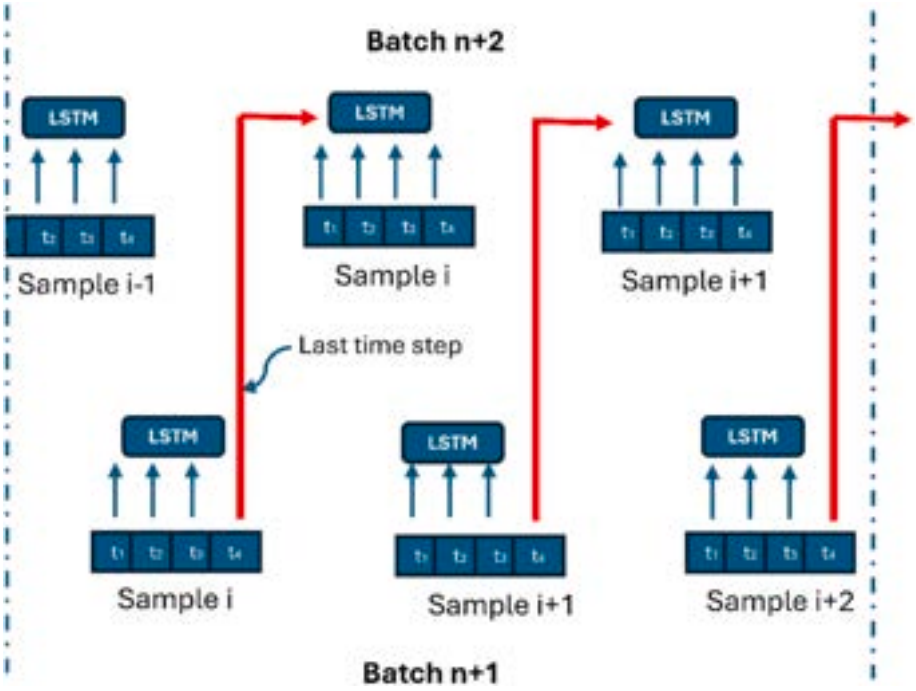

Fig. 5. Visual propagation between batches in a stateful LSTM architecture.

stateful LSTM, these states are instead carried over to the next batch, allowing the model to "remember" previous information and maintain the continuity of the sequence.

Furthermore, in the stateful network, the batches are organised in such a way that the temporal sequence is preserved. This means that the next batch contains the next sequence from the previous batch. A more fine-grained visualisation showing this propagation across the batches is shown below (Fig. 5).

Finally, for State Initialisation and State Reset, at the start of a new sequence or epoch, the LSTM states were reset, so as not to carry information between different sequences or between different training epochs.

3.1.3. Model output

The output of the model is a temporal sequence of maps of H_s, Tp and θ predicted for the next 24 h. Each forecast considers the initial meteorological and oceanographic and bathymetry conditions.

3.1.4. Layers and hyperparameters

The model uses a sequential network, in which the first layer is an LSTM with 64 memory units. This layer is designed to process long and complex time sequences, exploiting the ability of LSTMs to retain relevant information through extended time steps. The layer receives input with a specific time dimension, corresponding to the number of time steps and the number of features for each time step. To ensure that the entire time sequence is propagated to subsequent layers, the *return_sequences=True* argument is used, which ensures that the output of each time step is passed to the next layer (Graves, 2013).

Following this first layer, a second LSTM layer with 32 memory units was inserted, which reduces complexity while still maintaining a strong representation capability of temporal dependencies. Again, the *return_sequences = True* option was retained, allowing the model to transmit detailed information on temporal patterns to subsequent layers.

To prevent overfitting, a dropout layer was inserted at a rate of 20%. Dropout is a regular technique used to improve the model generalization, reducing the risk of the model overfitting the training data (Srivastava et al., 2014).

The third LSTM layer of the model consists of 16 memory units and it is designed to distill the information already processed in the previous layers into an even more compact representation. In this layer, the *return_sequences* option has not been activated, as the goal is to obtain a single output representing the final synthesis of the processed temporal information.

The final output is processed by a dense layer with eight neurons, selected to produce the predicted wave features. This number of neurons was chosen to adequately represent the outputs required by the model, providing a detailed prediction for each of the desired features.

The model was optimized using the Adam algorithm, which is known for its effectiveness in handling complex gradients in deep neural networks (Kingma, 2014). The learning rate was set at 0.001 to ensure gradual and stable learning, minimizing the risk of fluctuations during training. The model was trained for 40 epochs, with a batch size of 200, allowing the model's weights to be updated frequently, while still maintaining the stability required for training on complex data (Bengio, 2012).

3.1.5. Loss and optimization function

For training the model, a loss function based on the Mean Square Error (MSE) between predictions and observed values was used, which is one of the most common loss functions in regression problems (Chen et al., 2022; Martin-Donas et al., 2018), such as the prediction of marine parameters (wave height, period, direction). The MSE (Equation (7)) calculates the mean squares of the errors between the values predicted by the model and the actual values. More specifically, for each predicted value and the corresponding actual value, the error is squared and then the average of all these values is calculated. The MSE penalises larger errors, making it suitable for applications where it is important to minimise large deviations between prediction and reality (Port and Korte, 2008).

$$MSE = \frac{\left(\sum_{i=1}^{n} (x_i - \hat{x}_i)^2\right)}{n} \quad \text{(Eq. 7)}$$

Where xi is the i-th forecast and $x\hat{i}$ is the estimator.

Another metric estimated during the learning and validation processes is the Mean Absolute Error MAE, which is described in detail in

the following section.

3.1.6. Summary of model improvements and evaluation

After defining the model architecture, hyperparameters, and loss function, it is essential to contextualize our approach relative to existing methods, highlighting the improvements introduced in wave forecasting. Our model builds upon previous work by Fu et al. (2022) and Han et al. (2022), incorporating key advancements to enhance accuracy and generalization.

A major distinction lies in the handling of input data. By integrating wind and bathymetry data at a finer spatial resolution (4.6 km), our model captures local oceanic variations with greater precision. Additionally, the inclusion of RON buoy data for training and validation improves forecast reliability by grounding predictions in real-world observations.

Architecturally, we employ a deeper convolutional network with progressively increasing convolutional filters and 5 × 5 kernels, allowing for more detailed spatial feature extraction. This enhanced architecture strengthens the model's ability to learn complex wave patterns, improving generalization across diverse oceanic conditions.

For temporal sequence modeling, we leverage stateful LSTMs to preserve network states across training batches, ensuring a more effective capture of long-term dependencies such as seasonal variations and persistent meteorological influences.

To mitigate overfitting and improve robustness, we incorporate a 20% dropout rate as a regularization strategy. Additionally, the model is optimized using the Adam optimizer with a learning rate of 0.001, striking a balance between stability and efficient convergence.

Finally, our evaluation framework goes beyond standard RMSE metrics by also incorporating Mean Squared Error (MSE) and Mean Absolute Error (MAE), offering a more comprehensive assessment of predictive accuracy. The validation against RON buoy observations further ensures rigorous performance benchmarking against real-world conditions.

3.2. CMEMS-Conv-LSTM error metrics

The first error metric used to assess the performance of the model on case studies is the Mean Absolute Error (MAE). The MAE measures the mean absolute error between predicted and observed values. It is the average of the absolute differences between predicted and observed values. A MAE value of 0, indicates that there is no difference between the predicted and observed values. Lower values are better as smaller differences indicate minimal error. The MAE equation is shown below (Equation (8)).

$$MAE = \frac{1}{n}\sum_{i=1}^{n}|y_i - \hat{y}_i| \quad \text{(Eq. 8)}$$

With yi representing the actual value, $\hat{y}i$ the expected value and n the total number of observations.

The second metric is MAPE (Mean Absolute Percentage Error), which measures the mean absolute percentage error. It is the average of the absolute percentage differences between predicted and actual values. The MAPE equation is shown below (Equation (9)).

$$MAPE = \frac{100\%}{n}\sum_{i=1}^{n}\left|\frac{(y_i - \hat{y}_i)}{y_i}\right| \quad \text{(Eq. 9)}$$

The optimal MAPE value is 0%, which indicates a perfect match between predictions and observed values. Lower values indicate higher model accuracy. A MAPE value of less than 10% is generally considered very good in many contexts (Vivas et al., 2020).

The third metric, MASE (Mean Absolute Scaled Error), compares the mean absolute error of the model to the mean absolute error of a reference model, typically a naïve model. It is useful for comparing different models on different scales. The equation is shown below (Equation (10)).

$$MASE = \frac{\left(\frac{1}{n}\sum_{i=1}^{n}|y_i - \hat{y}_i|\right)}{\frac{1}{n-1}\sum_{i=2}^{n}|y_i - y_{i-1}|} \quad \text{(Eq.10)}$$

The optimal value of MASE is less than one, which indicates that the prediction model is better than the reference model. A MASE value of one means that the model is not better than the naïve model.

Finally, MDA (Mean Directional Accuracy), Equation (11), measures the percentage of times the model correctly predicts the direction of change (increase or decrease). It is a measure of directional accuracy.

$$MDA = \frac{1}{n}\sum_{i=1}^{n}1\left(\left(\frac{(y_i - y_{i-1})(\hat{y}_i - \hat{y}_{i-1})}{|y_i - y_{i-1}||\hat{y}_i - \hat{y}_{i-1}|}\right) > 0\right) \quad \text{(Eq.11)}$$

With 1 indicating the indicator function which is worth 1 if the condition is true, 0 otherwise.

A MDA value of 100% indicates that the model always correctly predicts the direction of change. Higher values are better and anything above 50% is considered better than a random prediction.

3.3. Accuracy metrics

To quantitatively assess the difference between the predictions of Conv-LSTM model and the reference data provided by CMEMS, two main statistical indicators are used: the BIAS and the Correlation Coefficient (CC). These two indices allow to characterise the accuracy and the correlation between simulated and observed values, respectively.

BIAS represents the average difference between simulated values H_s^{sim} and observed values H_s^{obs}, and it is defined as follows (Equation (12)).

$$BIAS = \frac{1}{n}\sum_{i=1}^{n}H_s^{sim}(i) - H_s^{obs}(i) \quad \text{(Eq.12)}$$

Where $H_s^{sim}(i)$ are the significant wave height values simulated by the Conv-LSTM or CMEMS model, $H_s^{obs}(i)$ are the values observed by buoys or other measuring instruments, and n is the number of observations.

A BIAS of zero indicates a perfect agreement between simulated and observed values, while a positive or negative BIAS indicates an over- or underestimation of wave heights by the model, respectively.

The Pearson correlation coefficient r or CC, on the other hand, measures the strength of the linear relationship between simulated and observed values, and is defined as follows (Equation (13)).

$$r = CC = \frac{\left(\sum_{i=1}^{n}\left(H_s^{sim}(i) - \overline{H}_s^{sim}\right)\left(H_s^{obs}(i) - \overline{H}_s^{obs}\right)\right)}{\sqrt{\left(\sum_{i=1}^{n}\left(H_s^{sim}(i) - \overline{H}_s^{sim}\right)^2\left(H_s^{obs}(i) - \overline{H}_s^{obs}\right)^2\right)}} \quad \text{(Eq.13)}$$

Where H_s^{sim} and H_s^{obs} are the averages of the simulated and observed values respectively, the other terms are as defined above.

The correlation coefficient ranges between −1 and 1, where 1 indicates a perfect positive correlation, 0 indicates no correlation, and −1 indicates a perfect negative correlation. A value of r close to 1 suggests that the model reproduces the observed pattern of wave heights well, while lower values indicate a poor ability to capture real patterns.

4. Results and discussion

4.1. Training and validation

Fig. 6 shows the trend of the training and validation results for the Conv-LSTM model. In particular, the loss and Mean Squared Error (MSE) values are plotted during both the training and validation phases.

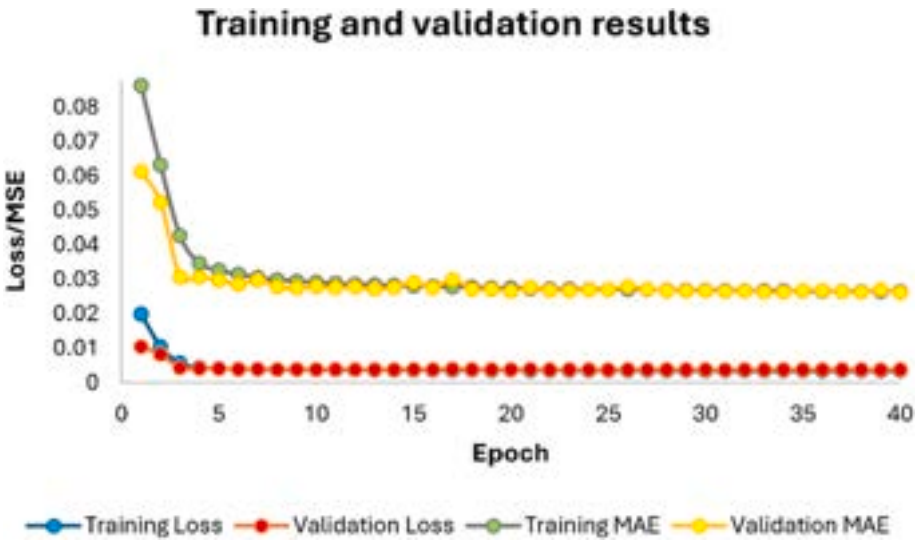

Fig. 6. Results of the training and validation processes of the Conv-LSTM model. The plot show either Loss and MAE results trough Epochs.

Fig. 6 shows the trend of Training Loss, Validation Loss, Training MAE, and Validation MAE as a function of epochs (up to 40) during the training of a model.

The y-axis in Fig. 6 represents the loss and MAE values, while the x-axis represents the number of epochs (up to 45). Training Loss is indicated by the blue line, Validation Loss by the red line, Training MAE by the grey line with green dots and Validation MAE by the yellow line.

At the beginning of the graph, the Loss values start with the Training Loss at around 0.078. Within a few epochs, the Training Loss decreases, stabilizing around the value of 0.008 already after the fifth epoch. The Validation Loss, which starts with a value very close to that of the Training Loss, undergoes similar behaviour and stabilizes around 0.008, suggesting that the model is not significantly overfitting, as the loss curves for training and validation are close and stable.

The Training MAE, represented by the grey line with green dots, starts at a value of around 0.088 and falls rapidly until it stabilizes around 0.028 after the tenth epoch. The Validation MAE also follows a similar behaviour, stabilizing just above 0.028 after a rapid initial drop.

The behaviour of the graph suggests that the model achieves good convergence, with similar values of training and validation for both loss and MAE. The absence of significant divergence between Training Loss and Validation Loss, as well as between Training MAE and Validation MAE, indicates that there is no obvious sign of overfitting, as the values remain close and stable after a few epochs.

4.2. *Mediterranean CMEMS-ConvLSTM application*

This section focuses on the comparison between Hs and Tp

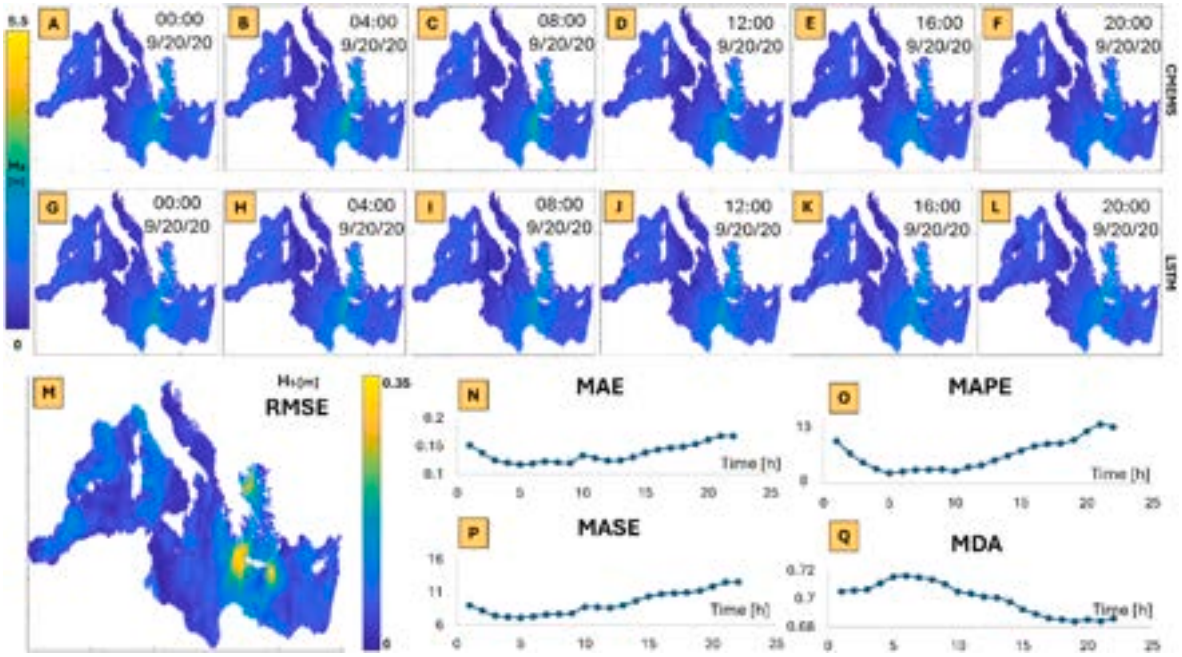

Fig. 7. Comparative results between CMEMS wave data (first row from top) and Conv-LSTM model predictions (second row from top) for *Hs* over the Mediterranean Sea on September 20, 2020, at different time intervals (00:00 Subplot A-G, 04:00 Subplot B-H, 08:00 Subplot C-I, 12:00 Subplot D-J, 16:00 Subplot E-K, 20:00 Subplot F-L). The bottom-left plot (Subploit M) shows the spatial distribution of the Root Mean Square Error (RMSE) between the two datasets. The time-series plots on the bottom right display the model's performance metrics: Mean Absolute Error (MAE) (Subplot N), Mean Absolute Percentage Error (MAPE) (Subplot O), Mean Absolute Scaled Error (MASE) (Subplot P) and Mean Directional Accuracy (MDA) (Subplot Q), evaluated over a 24-h period. The reference system used is EPSG:9834 - Mollweide to allow a distorted view of the entire Area considering the logitudinal and latitudinal axes equal.

predictions generated by the Conv-LSTM model and data provided by the Copernicus Marine Environment Monitoring Service (CMEMS) operational system for the Mediterranean Sea. The main objective is to assess the ability of the neural network-based model to produce satisfactory maps of H_s evolution over time and to compare them with CMEMS data, thus identifying strengths and weaknesses of the Conv-LSTM approach. Significant similarities in the spatial and temporal distribution of the waves were identified, as well as discrepancies that may affect operational predictions in real-world scenarios.

Fig. 7 (first and second rows, from subplots A to F and from subplot G to L, respectively) shows a comparison of the *Hs* predictions provided by two models, CMEMS (Copernicus Marine Environment Monitoring Service) and Convolutional Long Short-Term Memory (Conv-LSTM), for September 20, 2020. Fig. 7 is organised in a grid of eight panels for each model, with snapshots at 4-h intervals covering the entire day (00:00, 04:00, 08:00, 12:00, 16:00, 20:00).

The colour scale on the left varies from blue (indicated for *Hs* values close to 0 m) to yellow (for maximum *Hs* values up to 5.5 m). This range allows areas with different wave heights to be visually identified. In both models, the areas with the highest wave heights are mainly concentrated in the central part of the Mediterranean region, especially near the Greek archipelago and the island of Crete. These areas, shown in green/yellow, highlight wave heights ranging from about 2.5 to 5.5 m.

A detailed description of the spatiotemporal trend in Fig. 7, with reference to subplots A to L, is available in the Supplementary Materials, section A.

Both models predict a similar wave development during the day, with the highest heights concentrated in the central-eastern Mediterranean region (Greece) and a general decrease in wave heights towards the end of the day. The main differences are observed in the peak wave values. CMEMS tends to predict slightly higher wave heights than Conv-LSTM at almost all times of the day, especially during the night and afternoon hours (00:00 and 16:00). However, the general trends and spatial distribution of the waves are comparable between the two models, indicating that both models correctly capture the main dynamics of the marine phenomenon in question.

Fig. 7M shows the RMSE map for significant wave height (*Hs*) between Conv-LSTM and CMEMS predictions. This map, covering the Mediterranean, uses a blue-to-yellow scale (0–0.35 m). Most of the region shows low RMSE (<0.1 m), indicating strong agreement between models. Higher RMSE values (up to 0.35 m), shown in green and yellow, appear near the Greek coasts and Crete, where the models diverge the most. Overall, the models align closely across the Mediterranean.

Fig. 7N and Q presents the temporal evolution of four metrics used to evaluate the predictions of *Hs* between Conv-LSTM and CMEMS over the 24 h: Mean Absolute Error (MAE, Fig. 7N), Mean Absolute Percentage Error (MAPE, Fig. 7O), Mean Absolute Scaled Error (MASE, Fig. 7P), and Mean Directional Accuracy (MDA, Fig. 7Q).

MDA starts at approximately 0.1 m, remains stable until 12.00, and then increases to about 0.2 m by the end of the period, indicating growing discrepancies between the models. MAPE begins at around 13%, decreases to 8% in the morning, and returns to 13% by evening, reflecting a decline in the accuracy of Conv-LSTM relative to CMEMS. MASE follows a similar pattern, starting at approximately 6 and rising to about 16 later in the day, signifying increased error. Finally, MDA starts at 0.72, indicating high predictive accuracy, but decreases to about 0.68, suggesting again reduced ability to predict wave height changes in the evening hours.

Fig. 8 shows a comparison of the *Hs* predictions provided by the two models. In detail, in this figure, are shown the results obtained from the simulation of November 26, 2021.

Please, find a detailed description of the spatiotemporal trend in Fig. 8, with reference to subplots A to L, in the Supplementary Materials, section B.

Fig. 8M suggest, mainly in the Algerian coastal area, in the central Mediterranean, a larger discrepancy between the models in these areas. The remaining blue areas indicate a lower error, with better agreement between forecasts, in the Adriatic Sea and in the extreme eastern and western parts of the Mediterranean.

Fig. 8N shows that the average absolute error remains relatively stable throughout the day, with slight fluctuations around the value of 1.0. This indicates that, overall, the models maintain a constant mean error, with no major fluctuations at different times of day. MAPE (Fig. 8O), on the other hand, shows a percentage of absolute error

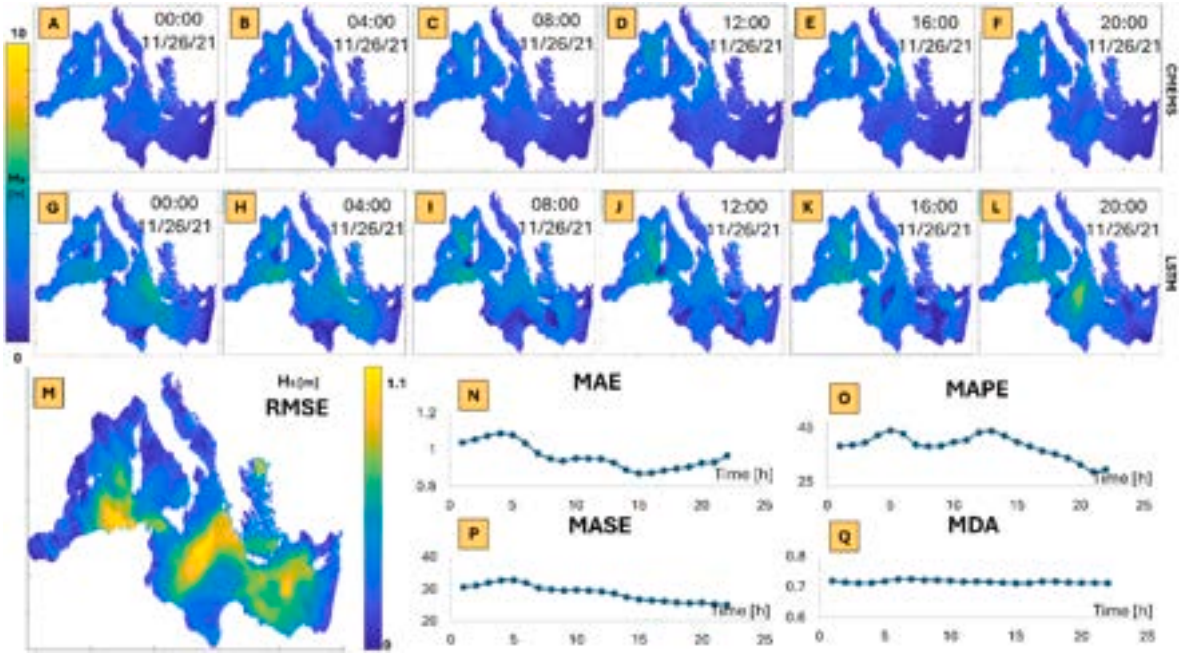

Fig. 8. Comparative results between CMEMS wave data (first row from top) and Conv-LSTM model predictions (second row from top) for *Hs* over the Mediterranean Sea on November 26, 2021, at different time intervals. The arrangement of the subplots in this figure follows the same structure as in Fig. 7. The reference system used is EPSG:9834 - Mollweide to allow a distorted view of the entire Area considering the logitudinal and latitudinal axes equal.

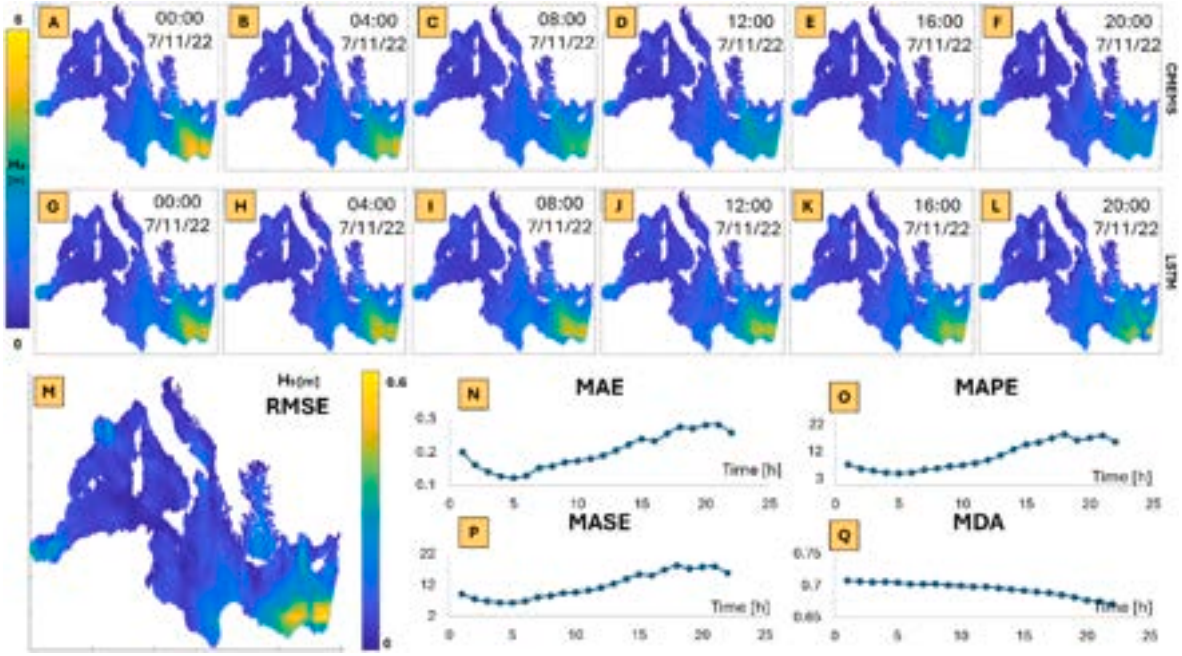

Fig. 9. Comparative results between CMEMS wave data (first row from top) and Conv-LSTM model predictions (second row from top) for *Hs* over the Mediterranean Sea on July 11, 2022, at different time intervals. The arrangement of the subplots in this figure follows the same structure as in Fig. 7. The reference system used is EPSG:9834 - Mollweide to allow a distorted view of the entire Area considering the logitudinal and latitudinal axes equal.

ranging between 30% and 45%. As for MASE (Fig. 8P), the graph shows a stable trend with values below 0.8. This value signals a good ability of the model to predict values with a proportionally small error. Finally, in the MDA (Fig. 8Q), a slight oscillation around the value of 0.7 is noted, indicating that most of the errors remain close to the median of the absolute errors, suggesting that the deviations do not diverge significantly from the central value, thus contributing to a uniform distribution of errors.

Fig. 9 presents the time series of simulations from November 07, 2022.

A detailed description of the spatiotemporal trend in Fig. 9, with reference to subplots A to L, is available in the Supplementary Materials, section C.

In the RMSE map, positioned at the bottom left (Fig. 9M), the regions with the highest RMSE (0.4–0.6 m) are concentrated along the southern coasts and in the eastern part of the Mediterranean. In contrast, much of the western Mediterranean has relatively low errors, with values below 0.2 m.

The plot of the MAE (Fig. 9N), shows that the metric starts from an initial value of about 0.12 m in the early hours of the day and gradually increases, reaching a maximum of 0.25 m. MAPE (Fig. 9O), starts at around 7 % in the early hours of the day and remains relatively stable. Then, it starts to increase and reaches a peak of about 13% around the evening. As for the MASE (Fig. 9P), it starts at about 6 in the early hours of the day and gradually increases until it reaches a value of 22 in the evening hours. Finally, the MDA (Fig. 9Q), shows an initial value of about 0.75, signaling a high accuracy in forecasting direction in the early hours of the day. This value gradually decreases over the course of the day, dropping to around 0.65 in the final hours.

In summary, all metrics show good agreement between the Conv-LSTM and CMEMS model forecasts in the early part of the day, with discrepancies becoming slightly larger in the evening hours, as evidenced by the progressive increase in error metrics (MAE, MAPE, MASE) and the decrease in directional accuracy (MDA). The southern coastal regions of the Mediterranean present the highest discrepancies, with RMSE values up to a maximum of 0.6 m.

The last forecast simulation of the Conv-LSTM model on CMEMS data is presented in Fig. 10 for 01/27/2022.

Please, find a detailed description of the spatiotemporal trend in Fig. 10, with reference to subplots A to L, in the Supplementary Materials, section D.

The RMSE map (Fig. 10M) clarifies and highlights the discrepancies between the two models' predictions in terms of wave heights, with a colour scale ranging from 0 to 0.3 m. The result confirms the smallest variations by showing the regions with the highest RMSE, with a maximum of 0.3 m, in the western part of the Mediterranean, especially along the southwest coast of Spain and in the Alborán Sea (between Spain and Morocco). These areas coincide with the highest wave areas in the last hours of the day, suggesting that the differences between the two models are greatest where the waves were most intense but at the end of the day. The RMSE is generally lower in the eastern and central areas, with values below 0.1 m.

In Fig. 10N of, the MAE remains constant around 0.12 m for most of the day, with a slight increase around 20:00, when it reaches about 0.15 m. The discrepancies between the two models are relatively stable over time for most of the day. MAPE (Fig. 10O) varies between 8% and 10% in the early hours, where it peaks at around 12%. Again, the Conv-LSTM model maintains reasonable accuracy in comparison with CMEMS. The MASE (Fig. 10P) remains relatively stable during the day, varying between 7 and 10. The scale of the discrepancies between the two models, therefore, does not change drastically over the course of the day, but the differences only become more evident in the last few hours. Finally, the MDA (Fig. 10Q) starts from a value around 0.72 in the early hours of the day and gradually decreases to around 0.68 in the evening. The accuracy in predicting the direction of changes in the waves throughout the day also follows the patterns of the other metrics.

Another parameter for comparison on the ability of Conv-LSTM to accurately predict the Mediterranean meteorological climate was the *Tp*. RMSE maps of *Tp* (between CMEMS and Conv-LSTM) were reported for the events discussed above and shown in Fig. 11.

The color scale on the left ranges from blue (low RMSE values) to yellow (high RMSE values), spanning 0.5–4.5 s. The maps illustrate the spatial evolution of peak period estimation error, highlighting geographical variations. On September 20, 2020 (Fig. 11A), RMSE

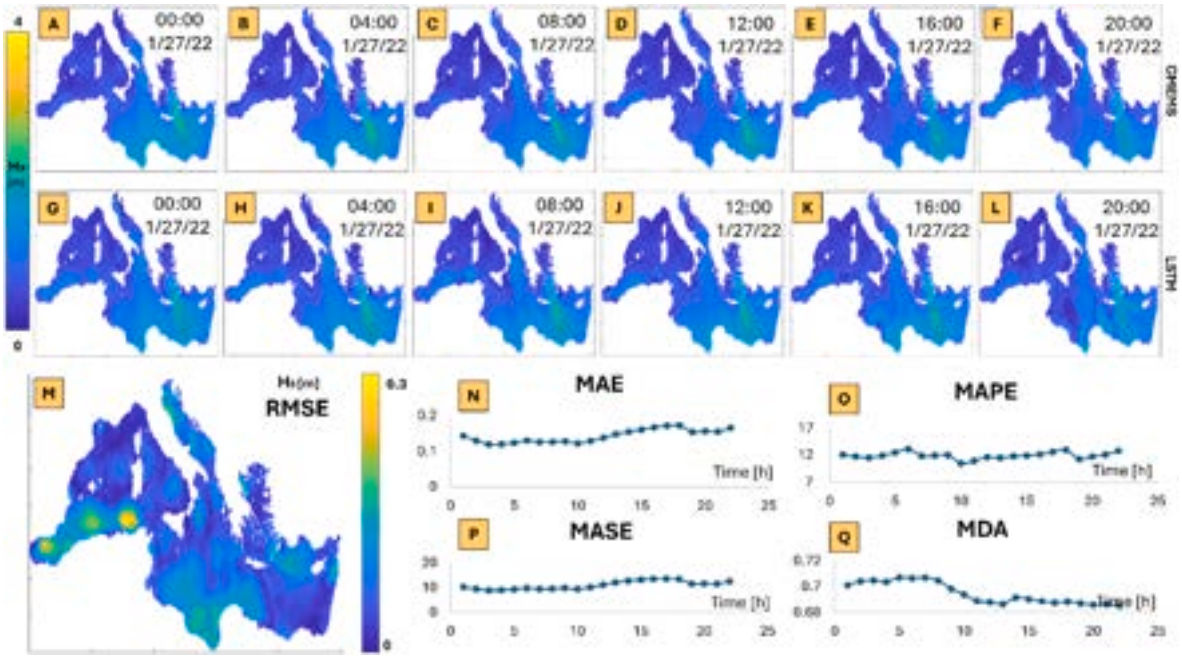

Fig. 10. Comparative results between CMEMS wave data (first row from top) and Conv-LSTM model predictions (second row from top) for *Hs* over the Mediterranean Sea on January 27, 2020, at different time intervals. The arrangement of the subplots in this figure follows the same structure as in Fig. 7. The reference system used is EPSG:9834 - Mollweide to allow a distorted view of the entire Area considering the logitudinal and latitudinal axes equal.

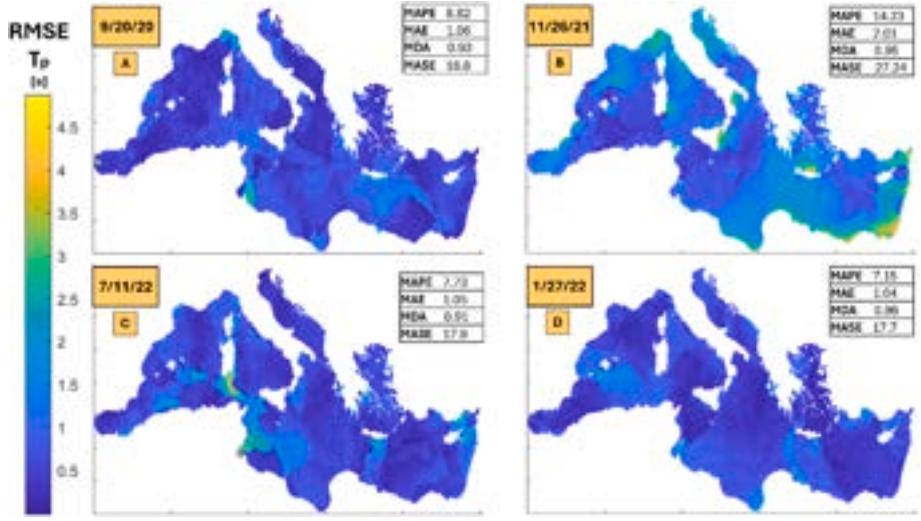

Fig. 11. Spatial distribution of RMSE for the peak period Tp [*s*] across the Mediterranean Sea, shown for all simulated events. The color scale represents the error magnitude in seconds. The statistical metrics MAPE, MAE, MDA, and MASE for each date are displayed in each date subplot (from A to D respectively for event 1 to 4 of Table 1). The reference system used is EPSG:9834 - Mollweide to allow a distorted view of the entire Area considering the logitudinal and latitudinal axes equal. (For interpretation of the references to colour in this figure legend, the reader is referred to the Web version of this article.)

values are generally low, with most of the Mediterranean in blue (error <2.5 s), while higher errors are concentrated along the northern and eastern coasts. Statistical indicators show a MAPE of 8.82, MAE of 1.06, MDA of 0.93, and MASE of 18.8, indicating good overall accuracy, particularly in coastal areas.

On November 26, 2021 (Fig. 11B), RMSE values increase significantly, particularly in the eastern and southeastern regions, reflected in a MAPE of 14.23, MAE of 2.01, MDA of 0.95, and MASE of 27.24, suggesting difficulties in predicting peak wave periods due to complex atmospheric conditions. By July 11, 2022 (Fig. 11C), errors decrease compared to the previous date, with central and western Mediterranean regions showing low errors, though some coastal areas still exhibit higher values. The indicators confirm this reduction: MAPE of 7.73, MAE of 1.05, MDA of 0.91, and MASE of 17.9, indicating a more uniform error distribution. Finally, on January 27, 2022, a similar pattern emerges with low RMSE values (below 1.5 s), but with further improvements, particularly in the southeastern Mediterranean. The statistical values are the lowest of all analyzed dates: MAPE of 7.15, MAE of 1.04, MDA of 0.96, and MASE of 17.7, indicating enhanced prediction quality over time, culminating in the best performance on this date.

Overall, the maps show significant spatial variability in the forecast error of the peak wave period, with marked differences between the dates considered. The highest errors are often associated with coastal areas and the eastern part of the Mediterranean Sea, where meteorological and oceanographic conditions may be more complex and difficult to model with the wind and bathymetric information layer alone. The

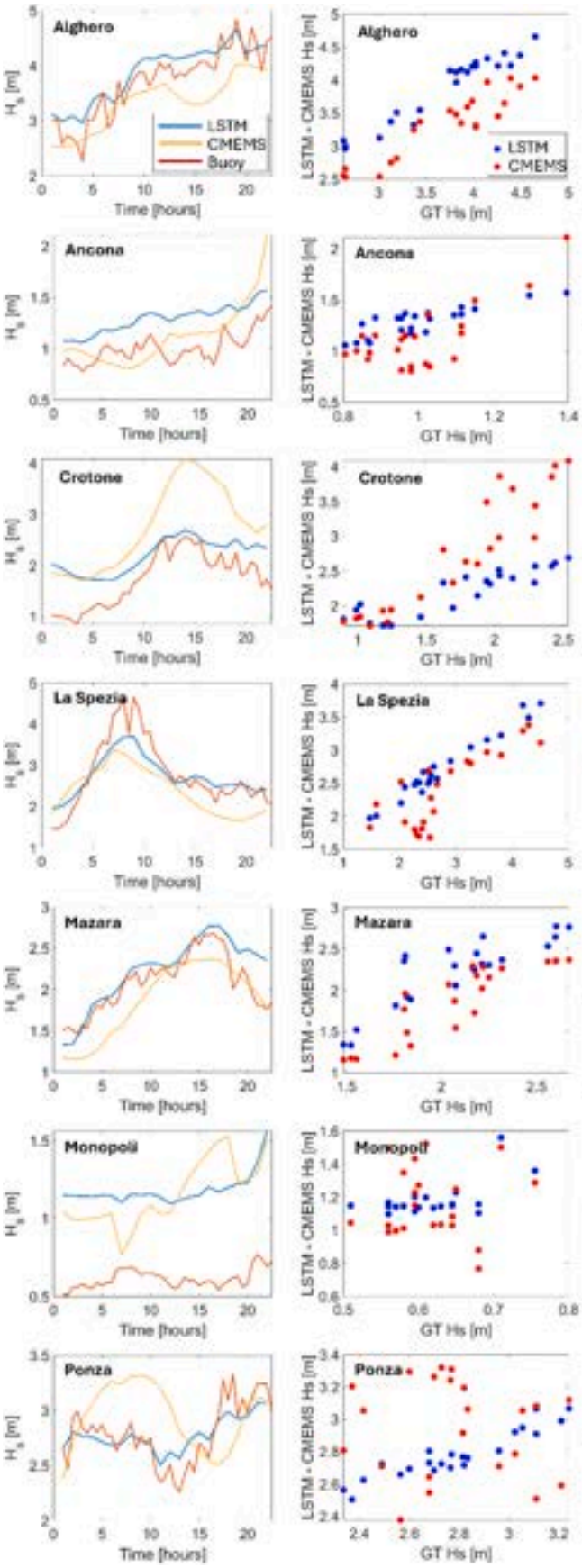

Alghero

MODEL	CC	BIAS
CMEMS	0.93	0.38
Conv-LSTM	**0.97**	**0.20**

Ancona

MODEL	CC	BIAS
CMEMS	0.75	**0.20**
Conv-LSTM	**0.85**	0.29

Crotone

MODEL	CC	BIAS
CMEMS	**0.93**	1.01
Conv-LSTM	0.90	**0.46**

La Spezia

MODEL	CC	BIAS
CMEMS	0.83	0.55
Conv-LSTM	**0.98**	**0.29**

Mazara

MODEL	CC	BIAS
CMEMS	**0.87**	0.25
Conv-LSTM	**0.87**	**0.17**

Monopoli

MODEL	CC	BIAS
CMEMS	0.05	**0.54**
Conv-LSTM	**0.59**	0.57

Ponza

MODEL	CC	BIAS
CMEMS	-0.09	0.36
Conv-LSTM	**0.93**	**0.11**

(caption on next page)

Fig. 12. The figure shows comparisons between Hs predictions using the Conv-LSTM model and the CMEMS dataset against RON buoy observations at various locations (Alghero, Ancona, Crotone, La Spezia, Mazara, Monopoli, and Ponza) for the 2 event (Table 1). The first columns display time series plots of Conv-LSTM (blue), CMEMS (yellow), and buoy data (red). The second columns show scatter plots comparing the predicted values from Conv-LSTM and CMEMS against buoy data. On the right, CC and bias values for each model are provided for each location. (For interpretation of the references to colour in this figure legend, the reader is referred to the Web version of this article.)

time evolution suggests an improvement in the forecasts, with a reduction in errors at later times.

Results on the comparison of simulated θ against CMEMS data are shown in the supplementary materials.

4.3. Validation RON buoy – CMEMS – ConvLSTM

In order to test the accuracy of the Conv-LSTM predictions and assess the magnitude of deviations from the CMEMS data, we compared for three different scenarios (2, 3 and 4 events of Table 1), the predictions obtained from the model with data from the Italian RON at 7 different locations in Italy (Alghero, Ancona, Crotone, La Spezia, Mazara, Monopoli and Ponza) as shown in section 2.2. The event 1 of Table 1 comparison is not provided because RON data are not available in 2020.

Fig. 12 shows three subplots for each location: (first column) the comparison between the data measured from the respective wave buoy (Buoy in red) and the predictions of the models (in yellow and blue for CMEMS and Conv-LSTM respectively); In the second column, the scatter plots between the values predicted by the models and those observed from the buoy (Ground Truth, GT). Finally, the third column shows the tables with the CC and the bias against the respective GT for the two models.

At several locations off the Italian coast, the comparative analysis between the Conv-LSTM and CMEMS models shows that the Conv-LSTM model offers more accurate predictions of *Hs*.

Conv-LSTM consistently outperforms CMEMS in wave height prediction, showing higher accuracy and lower dispersion across all locations. At Alghero and Ancona, Conv-LSTM follows observed data more closely, with CC values of 0.93 and 0.85, while CMEMS overestimates and oscillates more, with CCs of 0.63 and 0.75. In Crotone and La Spezia, Conv-LSTM captures wave peaks better, reaching CCs of 0.93 and 0.89, whereas CMEMS introduces oscillations not present in the real data. At Mazara and Monopoli, both models follow the trend well, but Conv-LSTM is slightly more precise in peak representation. Finally, at Ponza, Conv-LSTM shows the highest accuracy (CC = 0.93, bias = 0.11), while CMEMS performs poorly (CC = −0.06, bias = 0.39). The scatter plots confirm that Conv-LSTM consistently provides more reliable forecasts with less dispersion than CMEMS.

Overall, the results indicate that, at all locations analyzed, the Conv-LSTM model provides more accurate predictions than CMEMS, as confirmed by the higher correlation coefficients and lower bias. Conv-LSTM is particularly effective in capturing peak wave heights and has a lower dispersion than the observed data.

Fig. 13 also shows eight subplots arranged in three columns, illustrating the weather forecasts for the same locations as RON.

At Alghero, both models follow a similar trend, but CMEMS has slightly higher peaks. Conv-LSTM shows a stronger correlation (0.83 vs. 0.52) and a more concentrated scatter plot around the 1:1 line, with nearly identical biases (0.03 vs. 0.04). In Ancona, both models predict a rapid wave decrease, though CMEMS is closer to actual data. Conv-LSTM, despite a slight underestimation, has a higher correlation (0.69 vs. 0.56) and a lower bias (0.13 vs. 0.15). At Crotone, Conv-LSTM performs better, particularly in the second half of the day, with a correlation of 0.83 compared to CMEMS's 0.65 and a lower bias (0.12). In La Spezia, both models show a similar trend, but Conv-LSTM slightly overestimates in the later hours. Despite a higher correlation (0.88 vs. 0.79), Conv-LSTM also has a greater bias (0.09). At Mazara location, both models align well with observed data, though Conv-LSTM slightly overestimates in the early hours. It maintains a stronger correlation (0.87 vs. 0.74) but has a slightly higher bias (0.17 vs. 0.12). In Monopoli, both models underestimate initially, but Conv-LSTM overestimates later, showing greater dispersion. CMEMS has a lower correlation (0.27 vs. 0.65) but a significantly lower bias (−0.17 vs. 0.57). Finally, at Ponza, Conv-LSTM generally follows the observed trend but overestimates peaks. Despite its higher correlation (0.83 vs. 0.46), it exhibits greater dispersion in the scatter plot, with a similar bias (0.11).

In summary, the Conv-LSTM model shows a higher correlation with real data than CMEMS in almost all locations, proving to be more effective in capturing the general trend of wave heights. However, in this case, Conv-LSTM tends to overestimate in some regions, especially during peaks, while CMEMS appears more conservative, with a slight tendency to underestimate (behaviour already evidenced by Dodet et al., 2021; Ravdas et al., 2018; Sanchez-Arcilla et al., 2021).

Finally Fig. 14 also shows the same setup as the previous two (Figs. 12 and 13).

At Alghero, Conv-LSTM captures wave peaks more accurately, particularly around 5:00 and 18:00, with a higher correlation (CC = 0.83) and a lower bias (0.03) than CMEMS (CC = 0.42, bias = 0.05). In Ancona, Conv-LSTM better represents peaks, especially around hour 10, with a CC of 0.82 and a bias of 0.19, while CMEMS reaches a CC of 0.69 and a bias of 0.23. At Crotone, Conv-LSTM is significantly more accurate in capturing peaks, achieving a CC of 0.98 and a bias of 0.24, compared to CMEMS with a CC of 0.60 and a bias of 0.12. In La Spezia, Conv-LSTM provides a better representation of wave heights, particularly around hour 12, with a CC of 0.81 and a bias of 0.02, whereas CMEMS records a lower CC of 0.26 and a bias of 0.05. At Mazara, both models follow the general trend, but Conv-LSTM is more precise, with a CC of 0.84 and a bias of 0.09, compared to CMEMS (CC = 0.64, bias = 0.19). In Monopoli, Conv-LSTM better estimates peak heights, with a CC of 0.78 and a bias of −0.11, whereas CMEMS underestimates more, with a CC of 0.43 and a bias of 0.15. Finally, at Ponza, Conv-LSTM more accurately follows the wave pattern, achieving a CC of 0.40 and a bias of 0.08, while CMEMS performs poorly with a negative CC of −0.18 and a bias of −0.11.

The metrics clearly show the superiority of the Conv-LSTM model over CMEMS at all sites, with higher DC values and lower bias. At Ponza, CMEMS showed very poor performance, with a negative correlation coefficient, suggesting significant limitations of the model in calm conditions.

4.4. Comparison with previous approaches

This section aims to compare our Conv-LSTM model with previously proposed approaches to highlight key differences and improvements introduced by our work in the context of ocean condition forecasting in the Mediterranean Sea. The comparison emphasizes how our model is specifically designed to address the challenges related to the spatial and temporal variability of this region, optimizing predictive performance in operational scenarios.

Ding et al. (2023) and Jörges et al. (2023) applied a convolutional neural network (CNN)-based approach for ocean condition forecasting, primarily focusing on the classification of extreme events. While these models have shown promising results in detecting rare phenomena, they exhibit significant limitations in forecasting temporal dynamics, as they do not explicitly integrate time evolution. Our model, which combines the spatial feature extraction capabilities of CNNs with the long-term memory of LSTMs, addresses this gap by enhancing sequential prediction performance (Jörges et al., 2021). The integration of CNNs and LSTMs allows our model to better adapt to the variability of the

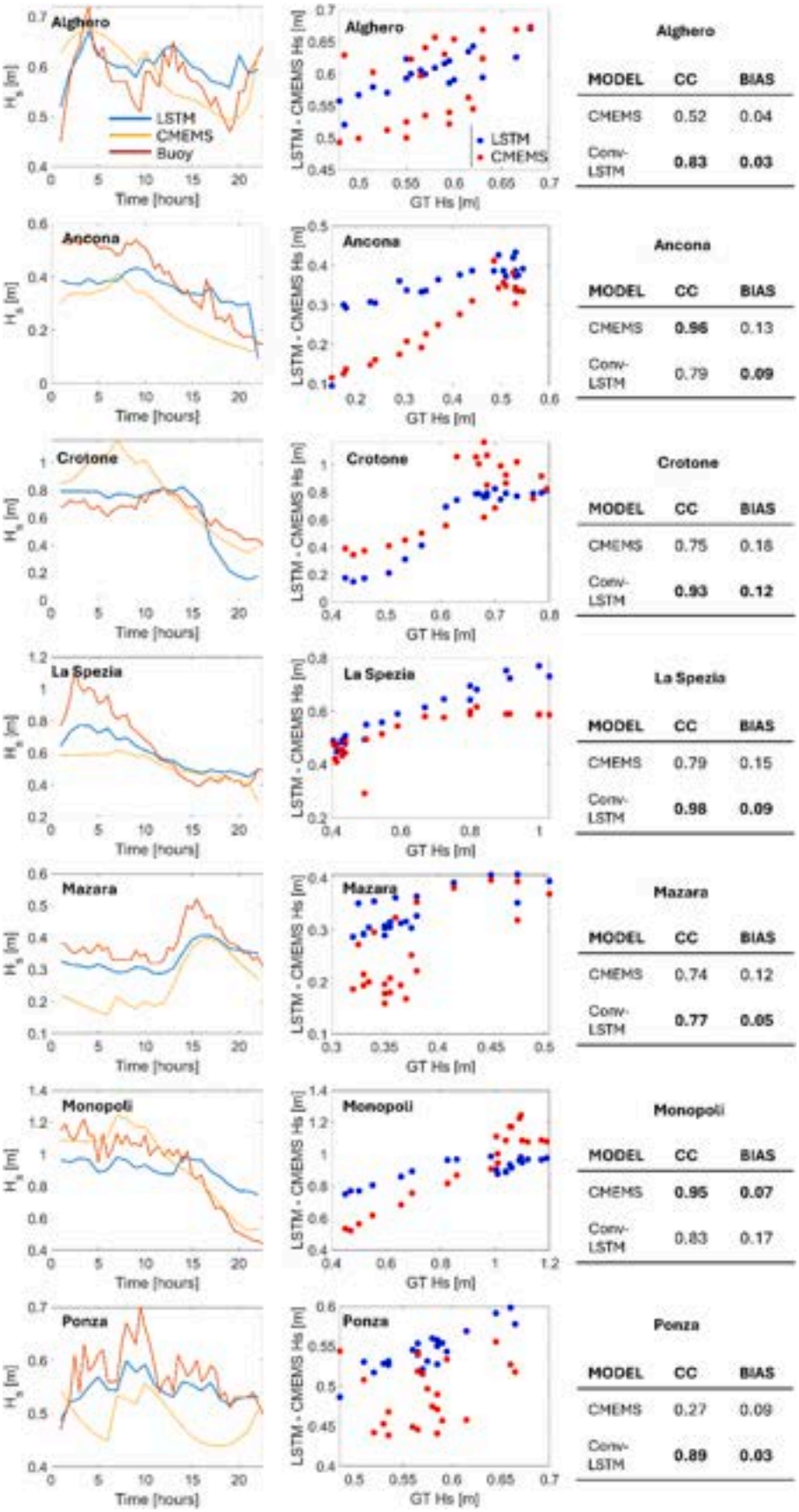

Alghero

MODEL	CC	BIAS
CMEMS	0.52	0.04
Conv-LSTM	**0.83**	**0.03**

Ancona

MODEL	CC	BIAS
CMEMS	**0.96**	0.13
Conv-LSTM	0.79	**0.09**

Crotone

MODEL	CC	BIAS
CMEMS	0.75	0.16
Conv-LSTM	**0.93**	**0.12**

La Spezia

MODEL	CC	BIAS
CMEMS	0.79	0.15
Conv-LSTM	**0.98**	**0.09**

Mazara

MODEL	CC	BIAS
CMEMS	0.74	0.12
Conv-LSTM	**0.77**	**0.05**

Monopoli

MODEL	CC	BIAS
CMEMS	**0.95**	**0.07**
Conv-LSTM	0.83	0.17

Ponza

MODEL	CC	BIAS
CMEMS	0.27	0.09
Conv-LSTM	**0.89**	**0.03**

Fig. 13. The figure shows comparisons between Hs predictions using the Conv-LSTM model and the CMEMS dataset against RON buoy observations at various locations (Alghero, Ancona, Crotone, La Spezia, Mazara, Monopoli, and Ponza) for the 3 event (Table 1). The arrangement of the subplots in this figure follows the same structure as in Fig. 12.

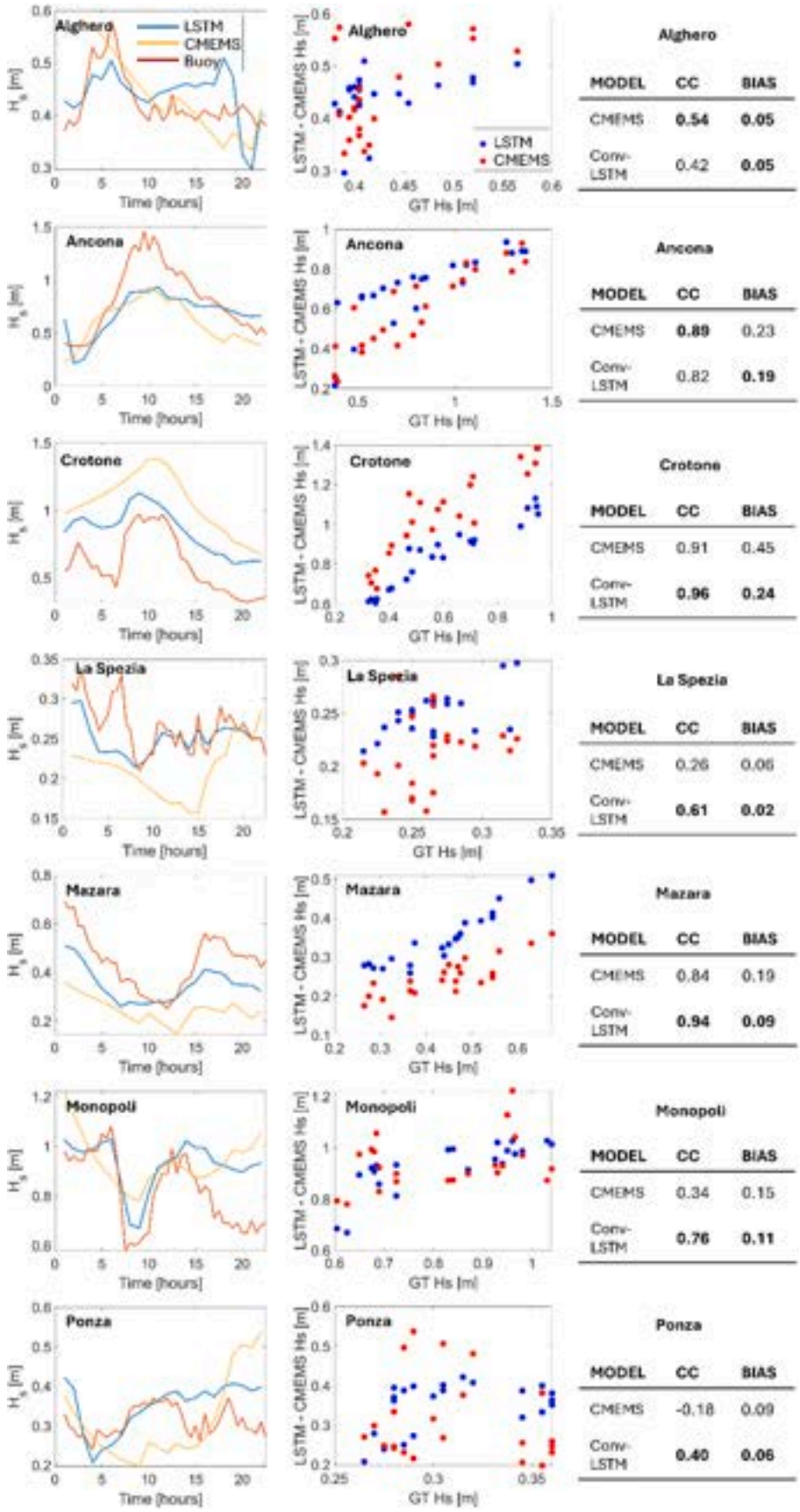

Alghero

MODEL	CC	BIAS
CMEMS	**0.54**	**0.05**
Conv-LSTM	0.42	**0.05**

Ancona

MODEL	CC	BIAS
CMEMS	**0.89**	0.23
Conv-LSTM	0.82	**0.19**

Crotone

MODEL	CC	BIAS
CMEMS	0.91	0.45
Conv-LSTM	**0.96**	**0.24**

La Spezia

MODEL	CC	BIAS
CMEMS	0.26	0.06
Conv-LSTM	**0.61**	**0.02**

Mazara

MODEL	CC	BIAS
CMEMS	0.84	0.19
Conv-LSTM	**0.94**	**0.09**

Monopoli

MODEL	CC	BIAS
CMEMS	0.34	0.15
Conv-LSTM	**0.76**	**0.11**

Ponza

MODEL	CC	BIAS
CMEMS	-0.18	0.09
Conv-LSTM	**0.40**	**0.06**

Fig. 14. The figure shows comparisons between Hs predictions using the Conv-LSTM model and the CMEMS dataset against RON buoy observations at various locations (Alghero, Ancona, Crotone, La Spezia, Mazara, Monopoli, and Ponza) for the 4 event (Table 1). The arrangement of the subplots in this figure follows the same structure as in Fig. 12.

Mediterranean, where conditions frequently change across different temporal scales.

Liu et al. (2024) developed a recurrent neural network (RNN)-based model designed for medium-term forecasting of oceanographic conditions. While traditional RNNs perform well in capturing temporal trends, they suffer from the well-known "vanishing gradient" problem, which hinders the learning of long-range dependencies. Our Conv-LSTM model is specifically designed to mitigate this issue through its hybrid structure, combining CNNs with LSTMs. The LSTM component effectively manages long-term dependencies, enabling our model to provide more stable and accurate forecasts than traditional RNNs, particularly for long-term predictions in the complex Mediterranean environment.

Finally, Shi et al. (2023) and Yue Liu et al. (2024) proposed a Transformer-based architecture for wave forecasting, leveraging the attention mechanism to enhance temporal sequence representation. While Transformers have demonstrated significant advantages in predictive performance across various applications, their high computational cost makes them less suitable for high-resolution operational forecasting, where computational speed is crucial. The Conv-LSTM model provides an optimal balance between accuracy and computational efficiency, making it particularly well-suited for real-time applications in the Mediterranean, where processing large datasets quickly is essential.

5. Final considerations

The simulations carried out highlight the effectiveness of the Conv-LSTM model in predicting weather and sea conditions in the Mediterranean, but at the same time reveal some limitations compared to the CMEMS data, mainly related to the geographical complexity and the atmospheric and physical dynamics of the region. Despite a good overall agreement between the Conv-LSTM simulations and the CMEMS data, the discrepancies are more pronounced in the coastal areas and in the eastern regions of the basin, suggesting that in these areas the accuracy of the model may be affected by local factors that are not adequately captured by the available spatial resolution and the application of wind and bathymetry maps alone. In particular, the results indicate that the Conv-LSTM model tends to overestimate wave heights, especially during peaks periods, probably due to the sequential nature of the Conv-LSTM neural networks, which may emphasize the effects of transient meteorological phenomena. In contrast, the more conservative CMEMS model tends to underestimate such peaks but proves to be more stable in the long term. This behavior suggests that the Conv-LSTM emerges in capturing short-term dynamics but may be less accurate during complex or extreme weather conditions, where the increase in error (e.g. in terms of RMSE and MAPE) becomes more apparent. Indeed, an important consideration that emerged is the geographical variability of errors. The central and western regions of the Mediterranean show higher accuracy, while the eastern and southern areas register higher errors, probably due to the greater atmospheric and oceanographic complexity of the eastern basin, characterised by more irregular currents and winds (Pinardi and Masetti, 2000; Robinson et al., 1991). The simulations of 20 September and November 26, 2021 showed, for example, showed a significant increase in error during more intense weather events, confirming the model's difficulty in correctly predicting waves in the presence of major atmospheric disturbances. On the other hand, the results of July 3, 2022 indicate that the model has improved its performance over time, achieving greater accuracy in more stable and predictable meteorological conditions.

The Conv-LSTM model proved particularly effective in the central Mediterranean in capturing both spatial and temporal dynamics, especially in regions characterised by complex interactions between wind, waves and bathymetry. The results obtained from the comparison of the Conv-LSTM simulations with the RON wave data show a clear preeminence of the Conv-LSTM model over CMEMS, particularly in its ability to capture wave height peaks and to maintain a higher correlation with the observed data. This performance is particularly evident in locations such as Alghero, La Spezia and Crotone, where the Conv-LSTM demonstrated higher accuracy and reduced dispersion. However, in some regions, such as Monopoli and Ponza, there is a tendency for Conv-LSTM to overestimate wave heights, especially during peaks, while CMEMS data proved more conservative but less accurate in general. Validation with RON dataset has shown that the coupled use of convolutional layers and data from accurate and appropriately calibrated measurement instrumentation can significantly improve prediction accuracy.

However, the absence of some critical variables, such as air temperature and atmospheric pressure, limits the model's ability to accurately predict weather and sea conditions in all circumstances. In fact, coastal areas suffer from the lack of detailed bathymetry, a critical aspect for accurately representing the phenomena that influence wave formation near the coast. The application of the Conv-LSTM model may indeed represent a major advance in short-term meteorological forecasting at the Mediterranean scale, but there is wide room for improvement, especially in coastal areas and under extreme weather conditions. For future developments, it is proposed to integrate additional meteo-marine variables, such as atmospheric pressure and temperature (sea and atmospheric), and to improve bathymetric resolution in coastal regions, to increase the accuracy and reliability of forecasts. Being able to have reliable forecasts of this type of data available on a day-to-day basis could allow for an increase in accuracy.

In conclusion, the use of a Conv-LSTM model for forecasting weather conditions proves to be particularly useful in multiple operational and research contexts. Accurate predictions of wave and sea conditions are essential to ensure safe navigation and to support offshore engineering interventions, such as the construction and maintenance of offshore infrastructure. A concrete example is lagoons areas, where critical decisions (such as the opening or closing of the MOSE system in Venice lagoon) (Alberti et al., 2023) are strictly dependent on reliable wave predictions. A Conv-LSTM model can also provide early warning of storm surges, enhancing the ability to respond to extreme events. In addition to operational forecasting, such models are effective tools for creating hindcast and forecast datasets, which are crucial for feeding propagation models, and for refining the results of existing hydrodynamic models. The ability to understand the specific impact of wind on meteo-marine events is a further advantage, allowing the atmospheric components that influence wave dynamics to be distinguished more accurately. Finally, in a context such as the Mediterranean, where there is a lack of adequate statistical distributions for the peak period (Tp) of waves (Cañellas et al., 2024; Cherneva et al., 2005; Isaacson et al., 1981; Muraleedharan et al., 2015), such a model offers a more accurate and reliable prediction, contributing to a better statistical inference of meteo-marine data and reducing uncertainty in long and short term analyses.

CRediT authorship contribution statement

P. Scala: Writing – review & editing, Writing – original draft, Visualization, Validation, Software, Methodology, Investigation, Formal analysis, Data curation, Conceptualization. **G. Manno:** Writing – review & editing, Validation, Supervision, Conceptualization. **E. Ingrassia:** Writing – review & editing, Writing – original draft, Formal analysis, Data curation, Conceptualization. **G. Ciraolo:** Writing – review & editing, Writing – original draft, Supervision, Conceptualization.

Declaration of competing interest

The authors declare that they have no known competing financial interests or personal relationships that could have appeared to influence the work reported in this paper.

Acknowledgements

This study was carried out within the RETURN Extended Partnership that received funding from the European Union Next-GenerationEU (National Recovery and Resilience Plan – NRRP, Mission 4, Component 2, Investment 1.3 – D.D. 1243 August 2, 2022, PE0000005).

Appendix A. Supplementary data

Supplementary data to this article can be found online at https://doi.org/10.1016/j.oceaneng.2025.120917.

References

Accarino, G., Chiarelli, M., Fiore, S., Federico, I., Causio, S., Coppini, G., Aloisio, G., 2021. A multi-model architecture based on Long Short-Term Memory neural networks for multi-step sea level forecasting. Future Gener. Comput. Syst. 124, 1–9.

Alberti, T., Anzidei, M., Faranda, D., Vecchio, A., Favaro, M., Papa, A., 2023. Dynamical diagnostic of extreme events in Venice lagoon and their mitigation with the MoSE. Sci. Rep. 13, 10475.

Azzopardi, B., Balzan, M.V., Cherif, S., Doblas-Miranda, E., dos Santos, M., Dobrinski, P., Falder, M., Hassoun, A.E.R., Giupponi, C., Koubi, V.V., 2020. Climate and environmental change in the Mediterranean basin–Current situation and risks for the future. First Mediterranean Assessment Report.

Barceló-Llull, B., Pascual, A., Ruiz, S., Escudier, R., Torner, M., Tintoré, J., 2019. Temporal and spatial hydrodynamic variability in the Mallorca channel (western Mediterranean Sea) from 8 years of underwater glider data. J. Geophys. Res. Oceans 124, 2769–2786.

Bengio, Y., 2012. Practical recommendations for gradient-based training of deep architectures. In: Neural Networks: Tricks of the Trade, second ed. Springer, pp. 437–478.

Bento, P., Pombo, J., Mendes, R., Calado, M., Mariano, S., 2021. Ocean wave energy forecasting using optimised deep learning neural networks. Ocean Eng. 219, 108372.

Bolaños-Sanchez, R., Sanchez-Arcilla, A., Cateura, J., 2007. Evaluation of two atmospheric models for wind–wave modelling in the NW Mediterranean. J. Mar. Syst. 65, 336–353.

Booij, N., Ris, R.C., Holthuijsen, L.H., 1999. A third-generation wave model for coastal regions: 1. Model description and validation. J. Geophys. Res. Oceans 104, 7649–7666.

Cañellas, B., Orfila, A., Méndez, F.J., Menéndez, M., Gómez-Pujol, L., Tintoré, J., 2024. Application of a POT model to estimate the extreme significant wave height levels around the Balearic Sea (Western Mediterranean). J. Coast Res. 50, 329–333.

Casaioli, M., Catini, F., Inghilesi, R., Lanucara, P., Malguzzi, P., Mariani, S., Orasi, A., 2014. An operational forecasting system for the meteorological and marine conditions in Mediterranean regional and coastal areas. Adv. Sci. Res. 11, 11–23.

Cavaleri, L., Abdalla, S., Benetazzo, A., Bertotti, L., Bidlot, J.-R., Breivik, Ø., Carniel, S., Jensen, R.E., Portilla-Yandun, J., Rogers, W.E., 2018. Wave modelling in coastal and inner seas. Prog. Oceanogr. 167, 164–233.

Cavaleri, L., Bertotti, L., Buizza, R., Buzzi, A., Masato, V., Umgiesser, G., Zampieri, M., 2010. Predictability of extreme meteo-oceanographic events in the Adriatic Sea. Q. J. R. Meteorol. Soc. J. Atmospheric Sci. Appl. Meteorol. Phys. Oceanogr. 136, 400–413.

Cavaleri, L., Fox-Kemper, B., Hemer, M., 2012. Wind waves in the coupled climate system. Bull. Am. Meteorol. Soc. 93, 1651–1661.

Chen, X., Yu, R., Ullah, S., Wu, D., Li, Z., Li, Q., Qi, H., Liu, J., Liu, M., Zhang, Y., 2022. A novel loss function of deep learning in wind speed forecasting. Energy 238, 121808.

Cherneva, Z., Petrova, P., Andreeva, N., Soares, C.G., 2005. Probability distributions of peaks, troughs and heights of wind waves measured in the black sea coastal zone. Coast. Eng. 52, 599–615.

Dakar, E., Fernández Jaramillo, J.M., Gertman, I., Mayerle, R., Goldman, R., 2023. An artificial neural network based system for wave height prediction. Coast. Eng. J. 65, 309–324.

Danovaro, R., Fanelli, E., Canals, M., Ciuffardi, T., Fabri, M.-C., Taviani, M., Argyrou, M., Azzurro, E., Bianchelli, S., Cantafaro, A., 2020. Towards a marine strategy for the deep Mediterranean Sea: analysis of current ecological status. Mar. Pol. 112, 103781.

Denaxa, D., Korres, G., Flaounas, E., Hatzaki, M., 2024. Investigating extreme marine summers in the Mediterranean Sea. Ocean Sci. 20, 433–461.

Ding, J., Deng, F., Liu, Q., Wang, J., 2023. Regional forecasting of significant wave height and mean wave period using EOF-EEMD-SCINet hybrid model. Appl. Ocean Res. 136, 103582.

Dodet, G., Bidlot, J.-R., Accensi, M., Alday, M., Abdalla, S., Piolle, J.-F., Ardhuin, F., 2021. Error estimation of buoy, altimeter, and model significant wave height from triple collocation technique. https://doi.org/10.5194/egusphere-egu21-14753.

Donnelly, J., Daneshkhah, A., Abolfathi, S., 2024. Forecasting global climate drivers using Gaussian processes and convolutional autoencoders. Eng. Appl. Artif. Intell. 128, 107536.

Ducournau, A., Fablet, R., 2016. Deep learning for ocean remote sensing: an application of convolutional neural networks for super-resolution on satellite-derived SST data. Presented at the 2016 9th IAPR Workshop on Pattern Recogniton in Remote Sensing (PRRS). IEEE, pp. 1–6.

Feng, Z., Hu, P., Li, S., Mo, D., 2022. Prediction of significant wave height in offshore China based on the machine learning method. J. Mar. Sci. Eng. 10, 836.

Fu, E., Zhang, Y., Yang, F., Wang, S., 2022. Temporal self-attention-based Conv-LSTM network for multivariate time series prediction. Neurocomputing 501, 162–173.

Ghasemirahni, H., Farshin, A., Scazzariello, M., Chiesa, M., Kostić, D., 2024. Deploying stateful network functions efficiently using large language models. Presented at the Proceedings of the 4th Workshop on Machine Learning and Systems, pp. 28–38.

Graves, A., 2013. Generating sequences with recurrent neural networks. ArXiv Prepr. ArXiv13080850. https://doi.org/10.48550/arXiv.1308.0850.

Group, T.W., 1988. The WAM model—a third generation ocean wave prediction model. J. Phys. Oceanogr. 18, 1775–1810.

Habib, M.A., Zarillo, G.A., 2024. Construction of a real-time forecast model with deep learning techniques for coastal engineering and processes: nested in a basin scale suite of models. J. Mar. Sci. Eng. 12, 1152.

Han, L., Ji, Q., Jia, X., Liu, Y., Han, G., Lin, X., 2022. Significant wave height prediction in the South China Sea based on the ConvLSTM algorithm. J. Mar. Sci. Eng. 10, 1683.

Hashmi, M.F., Ashish, B.K.K., Keskar, A.G., Bokde, N.D., Yoon, J.H., Geem, Z.W., 2020. An exploratory analysis on visual counterfeits using conv-lstm hybrid architecture. IEEE Access 8, 101293–101308.

Hewitt, H.T., Bell, M.J., Chassignet, E.P., Czaja, A., Ferreira, D., Griffies, S.M., Hyder, P., McClean, J.L., New, A.L., Roberts, M.J., 2017. Will high-resolution global ocean models benefit coupled predictions on short-range to climate timescales? Ocean Model. 120, 120–136.

Hu, P., Cheng, W., Xu, G., Han, Y., Yan, N., Wang, N., 2023. Prediction of buffeting responses of the thin plate under joint action of wave and wind using LSTM and transfer learning. Appl. Ocean Res. 134, 103514.

Isaacson, M., de, S.Q., MacKenzie, N.G., 1981. Long-term distributions of ocean waves: a review. J. Waterw. Port Coast. Ocean Div. 107, 93–109.

Jörges, C., Berkenbrink, C., Gottschalk, H., Stumpe, B., 2023. Spatial ocean wave height prediction with CNN mixed-data deep neural networks using random field simulated bathymetry. Ocean Eng. 271, 113699.

Jörges, C., Berkenbrink, C., Stumpe, B., 2021. Prediction and reconstruction of ocean wave heights based on bathymetric data using LSTM neural networks. Ocean Eng. 232, 109046.

Khan, M.A., Karim, M.R., Kim, Y., 2019. A scalable and hybrid intrusion detection system based on the convolutional-LSTM network. Symmetry 11, 583.

Kingma, D.P., 2014. Adam: a method for stochastic optimization. ArXiv Prepr. ArXiv14126980. https://doi.org/10.48550/arXiv.1412.6980.

Kokkos, N., Zoidou, M., Zachopoulos, K., Nezhad, M.M., Garcia, D.A., Sylaios, G., 2021. Wind climate and wind power resource assessment based on gridded scatterometer data: a Thracian Sea case study. Energies 14, 3448.

Komen, G., 1986. Activities of the WAM (wave modelling) group. Presented at the SUT Oceanology: Proceedings of an International Conference, SUT, pp. SUT–AUTOE.

Krestenitis, M., Androulidakis, Y., Krestenitis, Y., 2024. Deep learning-based forecasting of sea surface temperature in the interim future: application over the Aegean, Ionian, and Cretan Seas (NE Mediterranean Sea). Ocean Dyn. 74, 149–168.

Li, G., Zhang, Hao, Lyu, T., Zhang, Huaifeng, 2024. Regional significant wave height forecast in the East China Sea based on the Self-Attention ConvLSTM with SWAN model. Ocean Eng. 312, 119064.

Lionello, P., Malanotte-Rizzoli, P., Boscolo, R., 2006. Mediterranean Climate Variability. Elsevier.

Liu, Y., Huang, L., Ma, X., Zhang, L., Fan, J., Jing, Y., 2023. A fast, high-precision deep learning model for regional wave prediction. Ocean Eng. 288, 115949.

Liu, Yong, Lu, W., Wang, D., Lai, Z., Ying, C., Li, X., Han, Y., Wang, Z., Dong, C., 2024. Spatiotemporal wave forecast with transformer-based network: a case study for the northwestern Pacific Ocean. Ocean Model. 188, 102323.

Liu, Yue, Zhang, X., Chen, G., Dong, Q., Guo, X., Tian, X., Lu, W., Peng, T., 2024. Deterministic wave prediction model for irregular long-crested waves with Recurrent Neural Network. J. Ocean Eng. Sci. 9, 251–263.

Lloret, J., Turiel, A., Solé, J., Berdalet, E., Sabatés, A., Olivares, A., Gili, J.-M., Vila-Subirós, J., Sardá, R., 2022. Unravelling the ecological impacts of large-scale offshore wind farms in the Mediterranean Sea. Sci. Total Environ. 824, 153803.

Mariotti, A., Pan, Y., Zeng, N., Alessandri, A., 2015. Long-term climate change in the Mediterranean region in the midst of decadal variability. Clim. Dyn. 44, 1437–1456.

Martin-Donas, J.M., Gomez, A.M., Gonzalez, J.A., Peinado, A.M., 2018. A deep learning loss function based on the perceptual evaluation of the speech quality. IEEE Signal Process. Lett. 25, 1680–1684.

Muraleedharan, G., Lucas, C., Martins, D., Soares, C.G., Kurup, P., 2015. On the distribution of significant wave height and associated peak periods. Coast. Eng. 103, 42–51.

Neshat, M., Nezhad, M.M., Sergiienko, N.Y., Mirjalili, S., Piras, G., Garcia, D.A., 2022. Wave power forecasting using an effective decomposition-based convolutional Bi-directional model with equilibrium Nelder-Mead optimiser. Energy 256, 124623.

O'Donncha, F., Hu, Y., Palmes, P., Burke, M., Filgueira, R., Grant, J., 2022. A spatio-temporal LSTM model to forecast across multiple temporal and spatial scales. Ecol. Inform. 69, 101687.

Oppenheim, N.G., Wahle, R.A., Brady, D.C., Goode, A.G., Pershing, A.J., 2019. The cresting wave: larval settlement and ocean temperatures predict change in the American lobster harvest. Ecol. Appl. 29, e02006.

Ouyang, L., Ling, F., Li, Y., Bai, L., Luo, J.-J., 2023. Wave forecast in the Atlantic Ocean using a double-stage ConvLSTM network. Atmospheric Ocean. Sci. Lett. 16, 100347.

Pinardi, N., Masetti, E., 2000. Variability of the large scale general circulation of the Mediterranean Sea from observations and modelling: a review. Palaeogeogr. Palaeoclimatol. Palaeoecol. 158, 153–173.

Port, D., Korte, M., 2008. Comparative studies of the model evaluation criterions MMRE and PRED in software cost estimation research. Presented at the Proceedings of the

Second ACM-IEEE International Symposium on Empirical Software Engineering and Measurement, pp. 51–60.
Ravdas, M., Zacharioudaki, A., Korres, G., 2018. Implementation and validation of a new operational wave forecasting system of the mediterranean monitoring and forecasting Centre in the framework of the Copernicus marine environment monitoring Service. Nat. Hazards Earth Syst. Sci. 18, 2675–2695. https://doi.org/10.5194/nhess-18-2675-2018.
Robinson, A., Golnaraghi, M., Leslie, W., Artegiani, A., Hecht, A., Lazzoni, E., Michelato, A., Sansone, E., Theocharis, A., Ünlüata, Ü., 1991. The eastern Mediterranean general circulation: features, structure and variability. Dynam. Atmos. Oceans 15, 215–240.
Salhi, A., Benabdelouahab, S., Bouayad, E.O., Benabdelouahab, T., Larifi, I., El Mousaoui, M., Acharrat, N., Himi, M., Ponsati, A.C., 2021. Impacts and social implications of landuse-environment conflicts in a typical Mediterranean watershed. Sci. Total Environ. 764, 142853.
Sanchez-Arcilla, A., Staneva, J., Cavaleri, L., Badger, M., Bidlot, J., Sorensen, J.T., Hansen, L.B., Martin, A., Saulter, A., Espino, M., Miglietta, M.M., Mestres, M., Bonaldo, D., Pezzutto, P., Schulz-Stellenfleth, J., Wiese, A., Larsen, X., Carniel, S., Bolaños, R., Abdalla, S., Tiesi, A., 2021. CMEMS-based coastal analyses: conditioning, coupling and limits for applications. Front. Mar. Sci. 8, 604741. https://doi.org/10.3389/fmars.2021.604741.
Sartini, L., Besio, G., Cassola, F., 2017. Spatio-temporal modelling of extreme wave heights in the Mediterranean Sea. Ocean Model. 117, 52–69.
Scala, P., Manno, G., Ciraolo, G., 2024a. Semantic segmentation of coastal aerial/satellite images using Deep Learning techniques: an application to coastline detection. Comput. Geosci., 105704
Scala, P., Toimil, A., Álvarez-Cuesta, M., Manno, G., Ciraolo, G., 2024b. Mapping decadal land cover dynamics in Sicily's coastal regions. Sci. Rep. 14, 22222. https://doi.org/10.1038/s41598-024-73085-5.
Sherwood, C.R., Van Dongeren, A., Doyle, J., Hegermiller, C.A., Hsu, T.-J., Kalra, T.S., Olabarrieta, M., Penko, A.M., Rafati, Y., Roelvink, D., 2022. Modeling the morphodynamics of coastal responses to extreme events: what shape are we in? Ann. Rev. Mar. Sci 14, 457–492.
Shi, J., Su, T., Li, X., Wang, F., Cui, J., Liu, Z., Wang, J., 2023. A machine-learning approach based on attention mechanism for significant wave height forecasting. J. Mar. Sci. Eng. 11, 1821.
Shi, X., Chen, Z., Wang, H., Yeung, D.-Y., Wong, W.-K., Woo, W., 2015. Convolutional LSTM network: a machine learning approach for precipitation nowcasting. Adv. Neural Inf. Process. Syst. 28.
Song, T., Han, R., Meng, F., Wang, J., Wei, W., Peng, S., 2022. A significant wave height prediction method based on deep learning combining the correlation between wind and wind waves. Front. Mar. Sci. 9, 983007.
Srivastava, N., Hinton, G., Krizhevsky, A., Sutskever, I., Salakhutdinov, R., 2014. Dropout: a simple way to prevent neural networks from overfitting. J. Mach. Learn. Res. 15, 1929–1958.
Tintoré, J., Pinardi, N., Álvarez-Fanjul, E., Aguiar, E., Álvarez-Berastegui, D., Bajo, M., Balbin, R., Bozzano, R., Nardelli, B.B., Cardin, V., 2019. Challenges for sustained observing and forecasting systems in the Mediterranean Sea. Front. Mar. Sci. 6, 568.
Toimil, A., Losada, I.J., Nicholls, R.J., Dalrymple, R.A., Stive, M.J.F., 2020. Addressing the challenges of climate change risks and adaptation in coastal areas: a review. Coast. Eng. 156, 103611. https://doi.org/10.1016/j.coastaleng.2019.103611.
Tolman, H.L., 1991. A third-generation model for wind waves on slowly varying, unsteady, and inhomogeneous depths and currents. J. Phys. Oceanogr. 21, 782–797.
Upreti, K., Arora, S., Sharma, A.K., Pandey, A.K., Sharma, K.K., Dayal, M., 2023. Wave height forecasting over ocean of things based on machine learning techniques: an application for ocean renewable energy generation. IEEE J. Ocean. Eng. 49, 430–445.
Vivas, E., Allende-Cid, H., Salas, R., 2020. A systematic review of statistical and machine learning methods for electrical power forecasting with reported mape score. Entropy 22, 1412.
Wang, N., Wang, Y., Er, M.J., 2022. Review on deep learning techniques for marine object recognition: architectures and algorithms. Control Eng. Pract. 118, 104458.
Wang, Y., Wang, H., Zhou, B., Fu, H., 2021. Multi-dimensional prediction method based on Bi-LSTMC for ship roll. Ocean Eng. 242, 110106.
Wu, L., Breivik, Ø., Rutgersson, A., 2019. Ocean-wave-atmosphere interaction processes in a fully coupled modeling system. J. Adv. Model. Earth Syst. 11, 3852–3874.
Zhang, J., Luo, F., Quan, X., Wang, Y., Shi, J., Shen, C., Zhang, C., 2024. Improving wave height prediction accuracy with deep learning. Ocean Model. 188, 102312.
Zhang, X., Li, X., 2020. Combination of satellite observations and machine learning method for internal wave forecast in the Sulu and Celebes seas. IEEE Trans. Geosci. Rem. Sens. 59, 2822–2832.
Zheng, G., Li, X., Zhang, R.-H., Liu, B., 2020. Purely satellite data–driven deep learning forecast of complicated tropical instability waves. Sci. Adv. 6, eaba1482.
Zheng, Z., Ali, M., Jamei, M., Xiang, Y., Abdulla, S., Yaseen, Z.M., Farooque, A.A., 2023. Multivariate data decomposition based deep learning approach to forecast one-day ahead significant wave height for ocean energy generation. Renew. Sustain. Energy Rev. 185, 113645.
Zhou, X., Liu, Z., Wang, F., Xie, Y., Zhang, X., 2020. Using deep learning to forecast maritime vessel flows. Sensors 20, 1761.